Microbial Cell Factories

RESEARCH

Open Access

Harnessing the power of *Neobacillus niacini* AUMC-B524 for silver oxide nanoparticle synthesis: optimization, characterization, and bioactivity exploration

Shimaa H. El-Sapagh[1], Nessma A. El-Zawawy[1], Mostafa E. Elshobary[1*], Mohammed Alquraishi[2], Hossain M. Zabed[3] and Hoda S. Nouh[1]

Abstract

Background Biotechnology provides a cost-effective way to produce nanomaterials such as silver oxide nanoparticles (Ag_2ONPs), which have emerged as versatile entities with diverse applications. This study investigated the ability of endophytic bacteria to biosynthesize Ag_2ONPs.

Results A novel endophytic bacterial strain, *Neobacillus niacini AUMC-B524*, was isolated from *Lycium shawii* Roem. & Schult leaves and used to synthesize Ag_2ONPS extracellularly. Plackett–Burman design and response surface approach was carried out to optimize the biosynthesis of Ag_2ONPs (Bio-Ag_2ONPs). Comprehensive characterization techniques, including UV–vis spectral analysis, Fourier transform infrared spectroscopy, transmission electron microscopy, X-ray diffraction, dynamic light scattering analysis, Raman microscopy, and energy dispersive X-ray analysis, confirmed the precise composition of the Ag_2ONPS. Bio-Ag_2ONPs were effective against multidrug-resistant wound pathogens, with minimum inhibitory concentrations (1–25 µg mL^{-1}). Notably, Bio-Ag_2ONPs demonstrated no cytotoxic effects on human skin fibroblasts (HSF) in vitro, while effectively suppressing the proliferation of human epidermoid skin carcinoma (A-431) cells, inducing apoptosis and modulating the key apoptotic genes including Bcl-2 associated X protein (*Bax*), B-cell lymphoma 2 (Bcl-2), Caspase-3 (*Cas-3*), and guardian of the genome (*P53*).

Conclusions These findings highlight the therapeutic potential of Bio-Ag_2ONPs synthesized by endophytic *N. niacini* AUMC-B524, underscoring their antibacterial efficacy, anticancer activity, and biocompatibility, paving the way for novel therapeutic strategies.

Keywords Silver oxide nanoparticles, Endophytic bacteria, Biosynthesis, Antibacterial, Anticancer, Apoptosis, Gene expression

*Correspondence:
Mostafa E. Elshobary
mostafa_elshobary@science.tanta.edu.eg
[1] Department of Botany and Microbiology, Faculty of Science, Tanta University, Tanta 31527, Egypt
[2] Department of Community Health Sciences, College of Applied Medical Sciences, King Saud University, 11421 Riyadh, Saudi Arabia
[3] School of Life Sciences, Guangzhou University, Guangzhou 510006, Guangdong, China

Background

Nanomaterials are recognized and utilized in several fields such as medicine, environmental science, biofuels, and electrical engineering [1–3]. Researchers have documented remarkable biological properties of silver-containing compounds, including antibacterial [4, 5], antitumor [6], thrombolytic, antioxidant, anticoagulant [7], and larvicidal activities [8]. Nanoparticles have garnered significant interest across many research fields due to their significant tiny size and large surface [9, 10]. Silver oxide nanoparticles (Ag_2ONPs) are well-known as a prominent category of metals oxide NPs that have gained attention thanks to their extensive applications and potential uses. The relevance of these NPs lies in their ability to influence the physicochemical characteristics of several materials [11, 12]. Ag_2ONPs are much more popular in the fields of textiles, food production, electronics, construction materials, pharmaceuticals, antimicrobials, cosmeceuticals, and the paint industry [13]. Their extremely small dimensions along with their relatively large surface areas, contribute to their unique properties and versatility and make them appealing for many sectors.

Ag_2ONPs demonstrate significant antibacterial properties, making them effective against a broad range of pathogenic bacterial strains, including multidrug-resistant pathogens [4, 5]. This characteristic has led to their use in various medical and healthcare applications such as wound dressings, topical ointments, and medical device coatings. Additionally, their antitumor activity [6] has generated interest in the development of silver-based nanoparticles for cancer treatment and diagnostics.

Silver oxide nanoparticles are synthesized by electrochemical or thermochemical methods [14–16] as well as reactive sputtering techniques [17]. Nevertheless, these methods necessitate specialized apparatus and a diverse range of hazardous substances [18]. Green synthesis methods, particularly those utilizing microorganisms, have demonstrated greater stability than chemically synthesized methods. This is partly due to the organic coating on the surface of microorganisms [19, 20]. Indeed, bacterial cells are readily cultivable and broadly employed to produce several metallic NPs, such as silver [21], iron oxide [22, 23], gold [24], and zinc oxide [25]. Recently, few studies have examined the successful biosynthesis of silver oxide NPs using bacteria such as *Bacillus thuringiensis* [6, 26] and *Pseudomonas aeruginosa* [27]. However, the biogenic production of Ag_2ONPs using bacterial endophytes remains largely unexplored. Bacterial endophytes are defined as "bacteria that inhabit and colonize the living internal tissues of plants in a symbiotic relationship without causing any immediate, overt negative effects" [28].

The presence of these bacteria in plant tissues may explain their ability to create compounds with useful industrial and medical uses [29]. The medicinal plant *Lycium shawii* (Roem. & Schultalso), known as Arabian Boxthorn, is part of the Solanaceae or nightshade family [30]. Plants in the Solanaceae family are well known for contain high levels of various compounds, including phenolics, alkaloids, flavonoids, steroids, coumarins, terpenoids, and carotenoids [31]. Extracts from *Lycium shawii* leaves have many biological effects, such as the ability to fight cancer, bacteria, and free radicals. These characteristics have significant relevance in the pharmaceutical and nutraceutical industries [32].

While there have been a few reports on the synthesis of AgNPs from endophytic fungi found in the plant *Lycium shawii* [33], no previous studies have reported the biosynthesis of Ag_2ONPs using bacterial endophytes from this plant. Therefore, our study aimed to synthesize and fully characterize biogenic environmentally friendly Ag_2ONPs by utilizing the endophytic bacterium *Neobacillus niacini* AUMC-B524 isolated from *Lycium shawii*. The goal was to investigate these biologically derived Ag_2ONPs as novel, promising therapeutic agents with potential medicinal applications.

Results and discussion

Isolation and identification of Ag_2ONPs producing endophytic bacterium

In this study, eight different endophytic bacteria were isolated from the pharmaceutical plant *Lycium shawii* leaves. Initial screening showed that only isolate 5 could reduce $AgNO_3$ into Ag_2ONPs. Figure 1A displays the characteristics of the colony morphology of the selected isolate, which appeared as smooth brown colonies on an LB agar plate supplemented with 0.5 mM $AgNO_3$.

Furthermore, the molecular identification of this isolate was successfully achieved (Fig. 1B). 16S rDNA gene amplification yielded a sequence of 1267 bp for the isolated strain, confirming its identity as *Neobacillus niacini* AUMC-B524. The sequence has been deposited in GenBank under the accession number OR149495. BLAST analysis revealed that the neighboring phylogenetic tree relative to *Neobacillus niacini* AUMC-B524 is *N. niacini* NBRC15566, with a high sequence similarity of 98.66% (GenBank accession no. NR_133777). Although various studies have investigated the biosynthesis of Ag_2ONPs, to our knowledge, this is the first documentation reporting the biosynthesis of Ag_2ONPs using *Neobacillus niacini*.

Ag_2ONPs biosynthesis by *N. niacini*

In this study, the biosynthesis of Ag_2ONPs by *N. niacini* AUMC-B 524 was observed by changing the cell-free supernatant from watery yellow to reddish brown, suggesting the biosynthesis of Ag_2ONPs. UV–vis

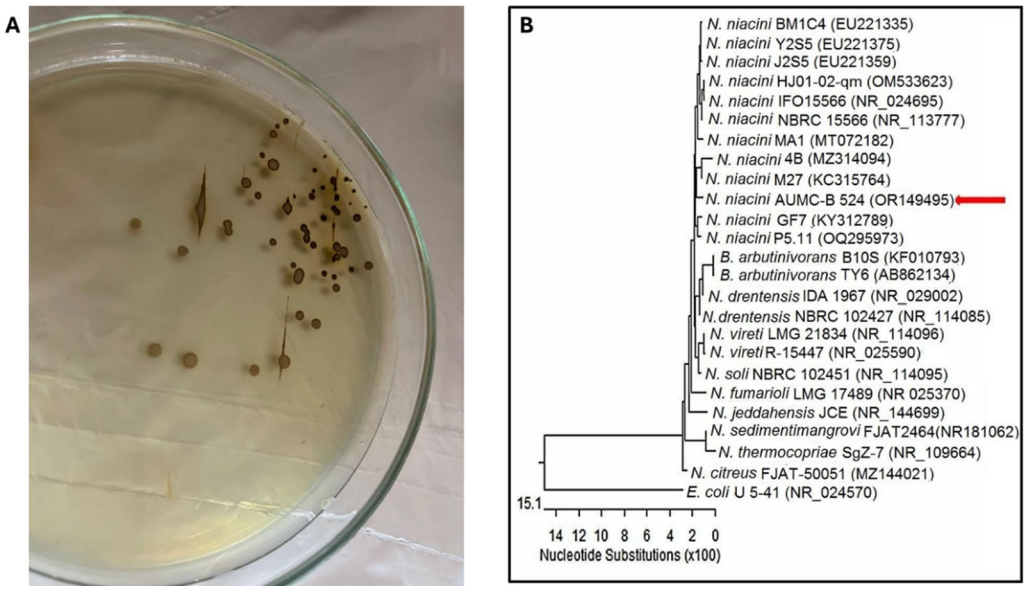

Fig. 1 Colony morphology with brown color on LB agar plate supplemented with 0.5 mM $AgNO_3$ (**A**), and the phylogenetic tree was constructed using 16S rDNA sequencing of *Neobacillus niacini* SH2 denoted by the arrow and aligned with other related sequences obtained from GenBank (**B**). This strain exhibited 98.66%–98.82% identity and 99%–100% coverage with various strains of *N. niacini*, involving the type material *N. niacin* NBRC15566 (GenBank accession no. NR_133777). The phylogenetic tree also included *E. coli* as an outgroup strain, denoted as E. for *Escherichia* and N. for *Neobacillus* (**B**)

spectroscopy displayed a prominent peak at 422 nm, which falls within the specifically defined range of Ag_2O NPs (Fig. 2). This peak is attributed to the surface plasmon resonance of nano-silver in the reaction mixture. Our results are harmonized with those documented by Manikandan et al. in their earlier investigation [34].

Optimization of Bio-Ag_2ONPs

The endophytic bacterium *N. niacini* AUMC-B 524 has demonstrated its potential to synthesize Ag_2ONPs. Efficient optimization of biosynthesis conditions is crucial for manufacturing these nanoparticles using a cost-effective methodology [35]. Using experimental design techniques for the optimization process offers advantageous results compared to the "one factor at a time" approach. Statistical experimental design approaches are more competitive and effective optimization strategies than the classic one-variable-at-a-time method [36]. In our optimization experiments, the initial stage involved conducting a rapid screening of biosynthesis factors to identify the components that substantially impact the manufacturing process of Ag_2ONPs. Plackett–Burman (PBD) design was employed in this study. This represents an economic methodology that identifies the primary impact of factors [37]. PDB is an effective two-factorial design applied to determine the critical factors that significantly affected Ag_2ONPs production process through experimental variable screening [38]. The best variables for optimizing the production of Ag_2ONPs from the cell-free supernatant of the *N. niciani* strain were defined using this approach. The biogenesis of Ag_2ONPs was assessed by quantifying the spectrophotometric absorbance at 422 nm. The Design-Expert software (Stat-Ease Inc. in Minneapolis, USA) was utilized to generate a statistically optimized set of twelve experimental runs aimed at evaluating which of the six factors under consideration had the most significant impact on the Ag_2ONP biosynthesis process. This experimental design facilitated the systematic screening and modeling of the key variables affecting Ag_2ONP production levels. The Plackett–Burman design (PBD) demonstrated a remarkable variation in the Ag_2ONPs yield in the twelve trials as the OD ranged from 0.61 to 1.99 at 422 nm (Table 1). These differences demonstrate the significance of optimizing these factors to enhance the production of Ag_2O nanoparticles.

The significance of each variable was conducted using P-values via ANOVA (Table S1). The obtained F-value of 26.58 indicates that the model exhibits statistical significance. P-values (Prob larger than F) below 0.05 indicate that the model terms were statistically significant.

The coefficient of determination (R_2) was used to assess the adequacy and fit of the model to the experimental data. The obtained R_2 value of 0.9696 indicates that the model could account for 96% of the variation observed in the response variables related to silver oxide nanoparticle (Ag_2ONP) production. This suggests the model provided

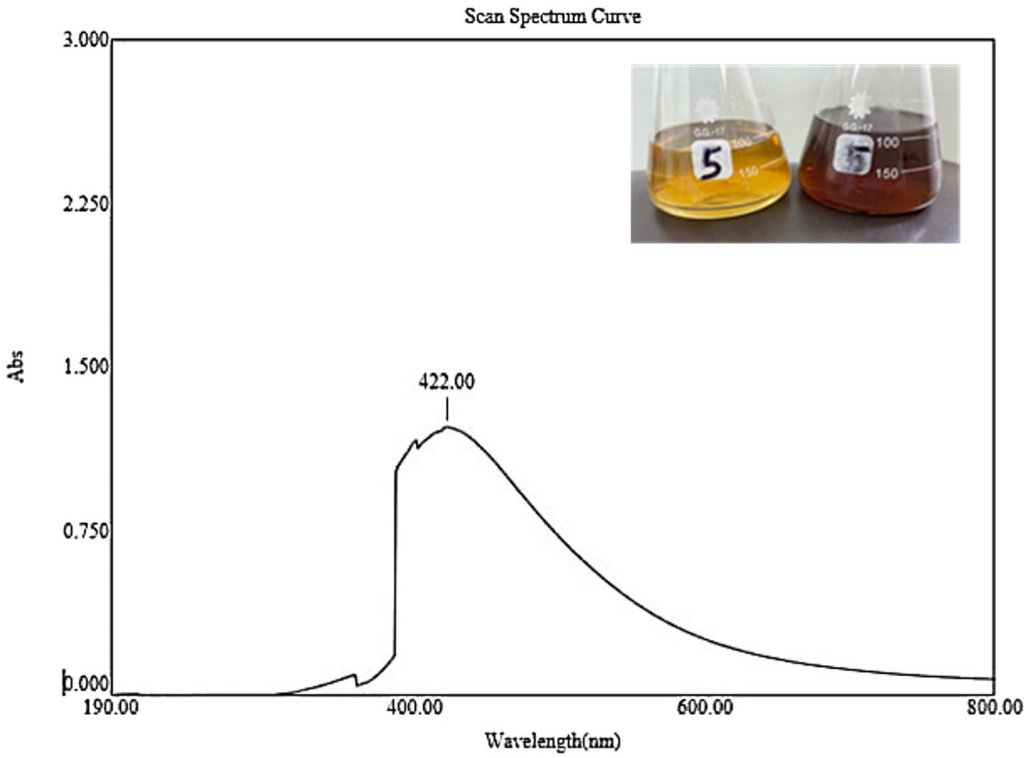

Fig. 2 UV–visible spectra of Bio-Ag_2ONPs using *N. niacini*. The Bio-Ag_2ONPs absorption was observed after 24 h of incubation and showed a distinct absorption peak at 422 nm

Table 1 Plackett–Burman experimental designs for the estimation of six independent variables for the biosynthesis of Ag_2ONPs by *Neobacillus niacini* strain AUMC-B524

Run no	Coded levels of independent variables											Ag_2ONPs yield ($OD_{422\,nm}$)	
	A	B	C	D	E	F	G	H	J	K	L	Actual value	Predicted value
1	+1	−1	+1	−1	−1	+1	−1	+1	+1	−1	+1	1.54	0.294
2	+1	+1	+1	+1	−1	−1	+1	−1	−1	−1	+1	1.9	0.059
3	+1	−1	−1	+1	+1	+1	+1	+1	−1	−1	−1	1.94	1.977
4	−1	−1	+1	+1	−1	+1	+1	−1	+1	+1	−1	1.63	1.155
5	−1	−1	+1	+1	+1	−1	−1	1	−1	+1	+1	0.88	0.059
6	−1	−1	−1	−1	−1	−1	−1	−1	−1	−1	−1	0.68	1.977
7	−1	+1	−1	+1	+1	+1	−1	−1	+1	−1	+1	1.89	0.02
8	+1	+1	+1	−1	+1	+1	−1	−1	−1	+1	−1	1.7	0.294
9	+1	−1	−1	−1	+1	−1	+1	−1	+1	+1	+1	0.89	1.116
10	+1	+1	−1	+1	−1	−1	−1	+1	+1	+1	−1	2	0.02
11	−1	+1	+1	−1	+1	−1	+1	+1	+1	−1	−1	0.74	0.881
12	−1	+1	−1	−1	−1	+1	+1	+1	−1	+1	+1	1.58	0.803

A: Bacterial supernatant, B: $AgNO_3$, C: pH, D: temperature, E: Reaction time, and F: illumination, G, H, J, K, L are dummy variables

a reliable estimation of the Ag_2ONP biosynthesis process in the present study.

Additionally, the adjusted R^2 value of 0.9331 was significant, further confirming the high relevance and fit of the model to the data. The calculated R^2 (0.8249) and adjusted R_2 (0.9331) values were in acceptable agreement with each other. This close alignment between the two R^2 values demonstrates the strong correlation between the experimentally observed results and the values predicted by the model.

The Ag_2ONPs synthesis plot (Fig. 3A) demonstrates the model's adequacy by indicating a strong accord between the actual experimental findings and the theoretical values anticipated by the model equation. The Pareto chart depicts the significance order of the variables that contribute to nanoparticle production [39]. The results

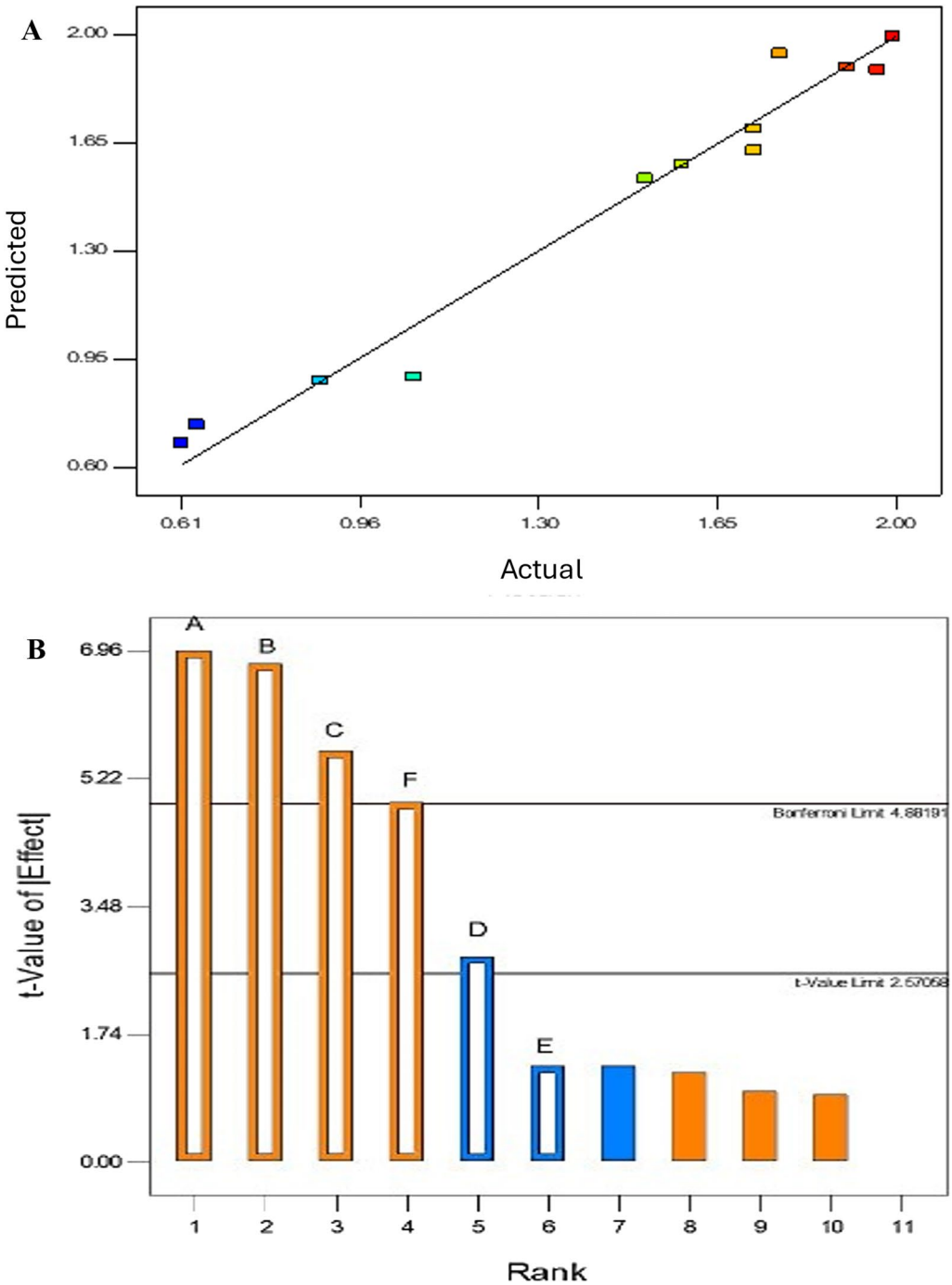

Fig. 3 The predicted and actual experimental value correlations for the Bio-Ag_2ONPs synthesis based on the results of the Plackett–Burman experimental design (**A**), which shows the degree of influence of each variable on the production of Bio-Ag_2ONPs (**B**). This chart indicates that the model consists of 11 variables (factors A, B, C, and F, represented by orange bars, demonstrate a significant relationship with the response. On the other hand, factors D and E, depicted by blue bars, have a significant negative relationship with the response. The other factors were not statistically significant

exhibited that the bacterial supernatant concentration, $AgNO_3$ concentration, pH, and light had a favorable impact on the synthesis of Ag_2ONPs (orange columns). Conversely, the temperature and reaction duration had a negative impact (blue columns) (Fig. 3B).

In this context, bacterial supernatant refers to the liquid portion obtained after centrifuging bacterial cultures. It can contain various biomolecules (phenolic, proteins, exopolysaccharides, etc.) that influence nanoparticle synthesis [40, 41].

Higher concentrations of bacterial supernatant may enhance Ag_2ONP formation due to the presence of reducing agents or stabilizers. $AgNO_3$ is commonly used as a silver precursor in nanoparticle synthesis. At low concentrations, it promotes nucleation and growth of Ag_2ONPs. However, too high a concentration can lead to aggregation or other undesired effects. Metallic silver on the nanostar spikes stabilizes their morphology, while excess silver deposits on the core and between neighboring spikes [42].

The behavior of particles undergoes changes in acidic and alkaline environments. However, the size of silver nanoparticles diminished as the pH increased within a given timeframe. In alkaline pH conditions, monodispersed, spherical nanoparticles were produced in greater quantities. At higher pH levels, the reaction rate accelerated, leading to the nucleation and growth of smaller-sized silver nanoparticles [43, 44]. Under basic pH conditions, there is lower aggregation, higher yield, faster growth, monodispersed distribution, and enhanced particle stability. Similarly, an increase in silver nitrate concentration results in particle aggregation [44, 45].

Light played a crucial role as the fourth major factor, acting as a photocatalyst in the process of reducing silver ions. While higher temperatures accelerate the reaction, they may also hinder the reducing agent's effectiveness. The synthesis progresses as time passes, eventually reaching a plateau when silver ions or reducing agents are depleted [46].

Concurrently with our research, Trivedi et al. [47] documented the optimization of five distinct variables of orange peel extracts. The Plackett–Burman design (PBD) was applied to examine the various variables that impact the production of AgNPs from citrus peel extracts. These factors include temperature, pH, reducing agent volume (reductant), illumination conditions, and silver nitrate precursor concentration.

Based on their findings, temperature had the greatest impact on the synthesis of AgNPs from citrus extracts, followed by illumination conditions and pH. However, silver nitrate precursor concentration appeared to have the lowest substantial effect on AgNP production among the studied factors. Halima et al. [48] used PBD to study factors affecting AgNP biosynthesis from betel of Piper and *Jatropha curcas* leaf extracts. In their findings, they showed that the extract of these plants, $AgNO_3$ concentration, and exposure to sunlight had the greatest impact on AgNPs biosynthesis.

The response surface methodology (RSM) was perofmed using a Box-Behnken design (BBD) technique to precisely identify the ideal levels of three choosen parameters (bacterial supernatant concentration, silver nitrate concentration, and pH value) to enhance the production process of biogenic silver oxide nanoparticles (Bio-Ag_2ONPs). The RSM integrates mathematical and statistical approaches to approximate and optimize a system's responses based on different experimental runs and multiple factors. It allows modeling and analysis to identify the conditions that maximize or minimize a particular response variable [49]. The study utilized response surface methodology to identify the specific values of the applied parameters necessary to achieve the desired response value within a restricted number of tests [50]. Baadhe et al. [51] technique was also employed to assess the interactions among the various parameters. The Box-Behnken design approach of the RSM has been widely recognized by researchers as a dependable and efficient instrument for optimizing and formulating various processes [52].

The BBD experiment was performed to explore the effects of three independent variables on Ag_2ONPs biosynthesis with a total of 17 experimental runs using different patterns of bacterial supernatant concentration (A), $AgNO_3$ concentration (B), and pH (C), as summarized in Table 2. Run 15 yielded the highest response, whereas run 11 resulted in the lowest response. The results obtained from the Box-Behnken experimental design were evaluated using ANOVA in Design Expert software. This was done to assess the statistical significance and qualification of the fitted response surface model [53]. Next, we used t-test analysis to estimate the statistical significance of the fitted polynomial model (Table S2). The ANOVA results displayed that the polynomial model was statistically significant, as evidenced by the Fisher's F-test value of 5.06 and a low probability value ($p = 0.0220$). These results imply that the model is acceptable and can precisely represent the true relationship between variables. The model's correlation coefficient (R^2) value was 0.8667, suggesting a strong correlation between the experimentally observed and model-predicted values. The adjusted R^2 value of 0.6953 implies that the model adequately justifies the response data variability. However, the predicted R^2 value of − 0.7578 indicates that using the overall mean may provide a better prediction of the response in this particular case.

Table 2 Box–Behnken design representing Ag_2ONPs production

Run No	Experimental parameters			Response Ag_2ONPs yield (O.D. at 422 nm)	
	A	B	C	Actual values	Predicted values
1	−1	−1	0	2.11	1.85
2	+1	−1	0	4.98	4.16
3	−1	+1	0	3.22	4.04
4	+1	+1	0	3.79	4.05
5	−1	0	−1	4.81	5.04
6	+1	0	−1	1.69	2.48
7	−1	0	+1	1.24	0.445
8	+1	0	+1	5.55	5.32
9	0	−1	−1	4.79	4.82
10	0	+1	−1	5.10	4.04
11	0	−1	+1	1.06	2.12
12	0	+1	+1	5.01	4.98
13	0	0	0	5.28	5.70
14	0	0	0	4.95	5.70
15	0	0	0	6.25	5.70
16	0	0	0	6.02	5.70
17	0	0	0	6.00	5.70

A quadratic polynomial equation that defines predicted response (R) was calculated by the model regression analysis as follows

$$R = 0.210196 + 0.179637 \times A + 0.0692517 \times B + 0.735833 \times C + -0.0164286 \times AB + 0.123833 \times AC + 0.173333 \times BC + -0.0142125 \times A^2 + -0.0615306 \times B^2 + -0.425 \times C^2 \quad (1)$$

where R is the predicted response and A, B, and C are coded for bacterial supernatant concentration, $AgNO_3$ concentration, and pH value, respectively.

To analyze the variables' interaction and define the optimum levels of each, 3D response surface plots along with 2D contour plots were generated (Fig. 4). On the z-axis of the 3D response surface plot, the yield or production level of the silver oxide nanoparticles was plotted (Fig. 4A, B, and C). In these 3D plots, two independent variables were varied concurrently, whereas the third variable was fixed at a coded value of zero, representing an intermediate level. The morphology of the counterplot functions as an indicator of the statistical significance of the interactions among independent variables [54]. Notably, variables A and C had a significant level of interaction, and the contribution of the correlation among other variables was limited. However, by employing numerical optimization techniques within the BBD framework, the optimal conditions and levels of the key factors were determined to maximize the production yield of the Ag_2ONPs. These settings included a bacterial supernatant concentration of 32.5%, 5.77 mM of $AgNO_3$, and a pH value of 6.77 (Fig. 5).

In a comparable investigation, RSM methodology was employed to optimize the efficiency of silver nanoparticles that were combined using the ethanolic plant extract from *Lepechinia meyenii* [55]. The results indicated that the most optimal parameter values were a high temperature of 49.8 °C, a basic pH of 9.45, an ethanolic fraction of 152.6 µL, and an incubation time of 213.2 min. In this study, the ideal pH for silver oxide nanoparticle synthesis was 6.77. These results align with the findings of Abdelmoneim et al. [39], where the ideal pH for producing AgNPs by using a liquid portion of *Leclercia adecarboxylata* THHM was 7. In our study, the bacterial supernatant concentration had a significant effect on the production of silver oxide nanoparticles, as the supernatant contains reducing agents. Followed by, $AgNO_3$ concentration as it contributes to the silver ions for Ag_2ONPs synthesis, followed by pH as pH influences the size and shape of nanoparticles and also impacts the biosynthetic process.

Characterization of Bio-Ag_2ONPs

Fourier transform infrared spectroscopy (FTIR)

In this study, we conducted FTIR spectroscopy analysis was performed to identify the functional chemical groups present in the biomolecules that contributed to the biosynthesis of Ag_2ONPs. The FTIR data provided insights into the biomolecules involved in reducing and stabilizing the Ag_2ONPs, influencing their reactivity and stability [56]. The resulting FTIR spectrum of the biosynthesized Ag_2ONPs (Bio-Ag_2ONPs), shown in Fig. 6A, exhibited four major absorption peaks in the wavenumber region of 400–4000 cm^{-1}. Specifically, the broad peak observed at 3448.70 cm^{-1} was assigned to the OH stretching vibrational modes, which is characteristic of alcohols or phenolic compounds present in the sample [57]. This suggests that alcohols and/or phenolic groups from the biomolecules were likely involved in the bioreduction and capping of the Ag_2ONPs during their biosynthesis, contributing to their formation and stability. These hydroxyl groups can form hydrogen bonds with the metal surface and render them hydrophilic, which affects their dispersibility and interactions with other molecules. The recorded peak at 2098.37 cm^{-1} implies the binding affinity of Ag^+ ions to nitrile or nitrite C≡N groups, which are known to be good ligands for metal nanoparticles and stabilize them against aggregation or degradation [58]. Moreover, the peak at 1641.56 cm^{-1} represents carbonyl C=O stretching and N–H bending vibration in the amide group, which is generally found in proteins [59]. Finally, the peak at 480.57 may be attributed to CH bending vibrations [60]. The findings of our study were comparable with the results of Sultan et al. [61], who observed

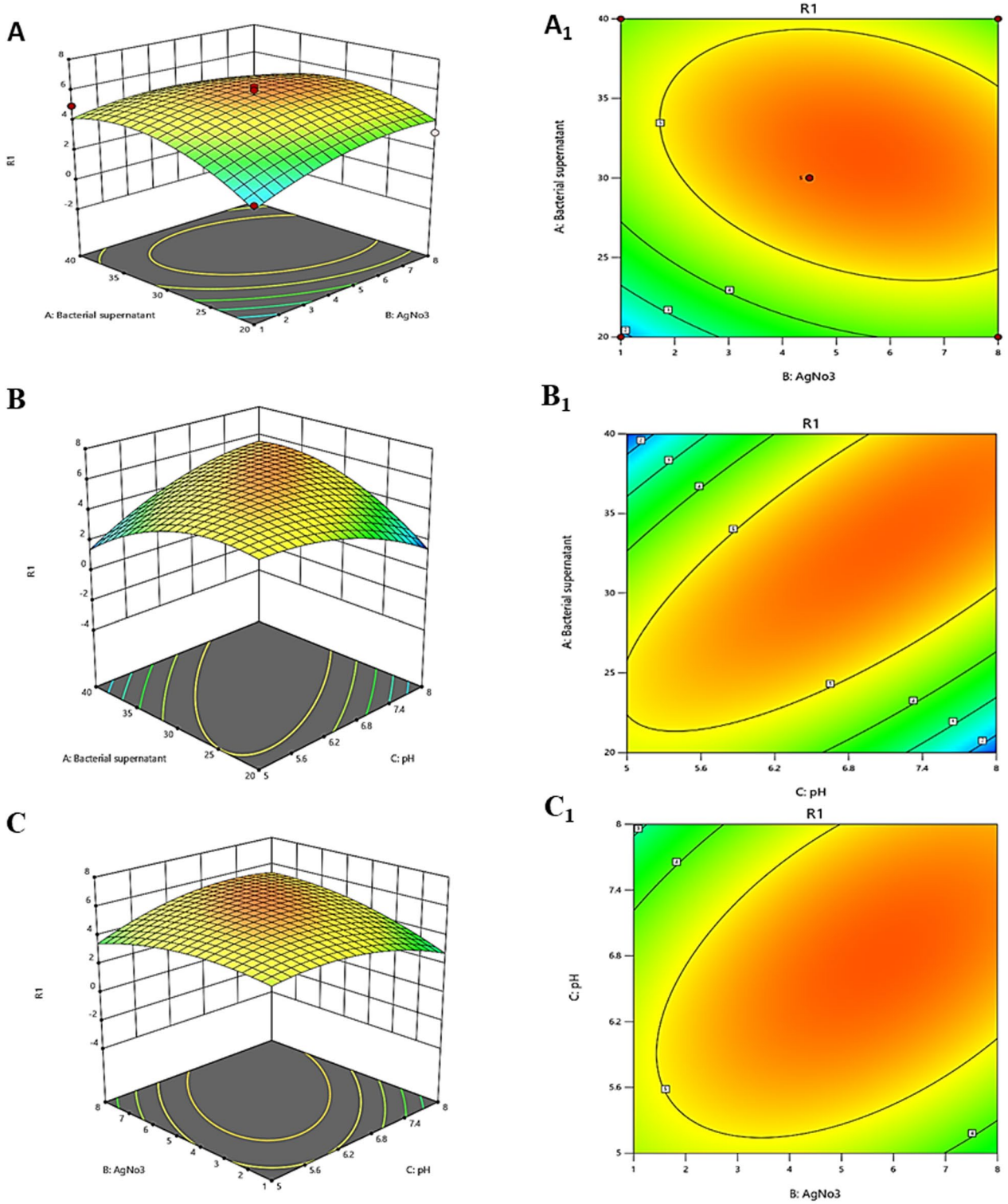

Fig. 4 The 3D surface response and contour plots reveal the influence of the bacterial supernatant concentration (**A**, **A1**), $AgNO_3$ concentration (**B**, **B1**), and pH value (**C**, **C1**) on Bio-Ag_2ONPs synthesis

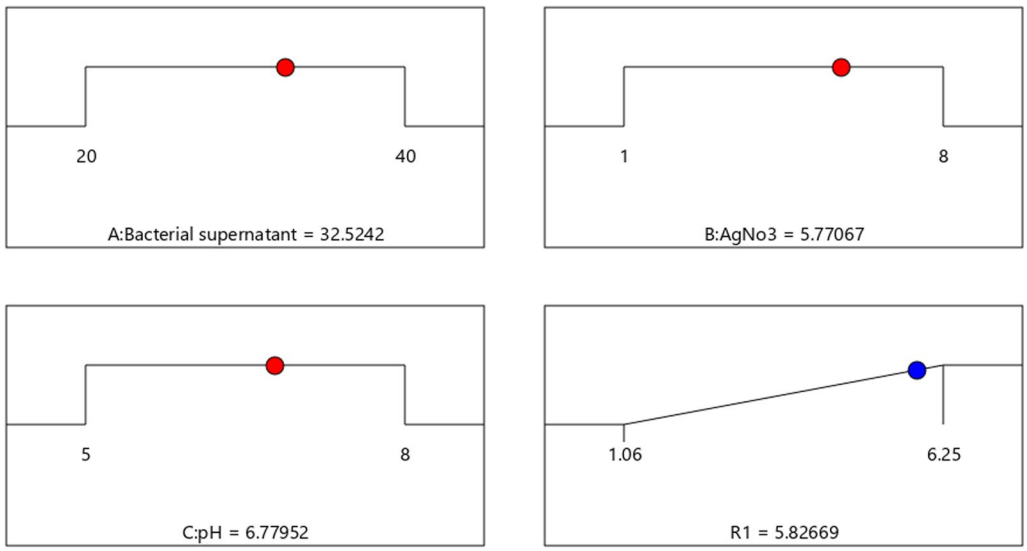

Fig. 5 The conditions for maximizing the Bio-Ag_2ONPs production following the BBD numerical optimization method

a similar peak trend in the FTIR spectrum of Ag_2O NPS synthesized using orange leaf extract.

Transmission electron microscope (TEM)

Further insight into the size and shape of the Bio-Ag_2ONPs, particles were analyzed using TEM. TEM micrographs revealed the formation of spherical and mono-distributed Ag_2ONPs without aggregation (Fig. 6B). This could be attributed to the presence of the coating and stabilizing agents [62]. The synthesized particle diameters ranged from 6.44 to 18.8 nm. A histogram depicting the distribution of particle sizes, derived from the TEM micrograph data, is presented in Fig. 6C. 45.4% of the Ag_2ONPs fall within the diameter of 10 to 15 nm, while the average particle size of bio-Ag_2ONPs was 13.16 nm. A previous study employed a similar methodology to characterize the size and shape of AgNPs biosynthesized from *Novosphingobium* sp. THG-C3, and *Sphingobium* sp. MAH-11T [63, 64].

Dynamic light scattering (DLS) and zeta potential measurements

The particle size of Ag_2ONPs was 94.3 ± 1.54 nm as estimated by dynamic light scattering with a zeta potential of − 14.87 ± 1.54 mV and a polydispersity index (PDI) of 0.26 ± 0.064 (Fig. 7A and B). The results indicated good quality and narrow size distribution of all the Bio-Ag_2ONPs with absorbed bioactive molecules on the particle surface. The greater negative zeta potential values confirmed the repulsion among the particles, which enhanced the polydispersity of the nanoparticles and prevented agglomeration, leading to the concise stability of the biosynthesized Ag_2ONPs [65].

The poly-dispersed nature of the nanoparticles is attributed to the highly negative zeta potential, which prevents the formation of agglomerates, leading to enhanced stability. The obtained nanoparticles exhibit a zeta potential of − 14.87 ± 1.54 mV (Fig. 7A and B), indicating the repulsive nature of the silver nanoparticles, contributing to their stability As the zeta potential approaches − 30 mV, the metal nanoparticles become more stable, and their harmful effects on biological systems are reduced [66]. Both negatively charged and small-sized nanoparticles with moderate to good stability (zeta potential from − 14.7 to 18.0 mV) and high stability (− 35.3 to − 81.5 mV) synthesized by bacteria have been reported by numerous research, aligning with our findings. However, variations in nanoparticle size and charge might be related to strain specificity and the growth conditions of the strain.

AgNPs are considered stable when their zeta potential exceeds + 30 mV or is below − 30 mV [67], as this charge range prevents agglomeration through repulsion. SEM analysis revealed spherical silver oxide nanoparticles with an average size of 45.39 nm, though some agglomeration was observed. This clustering is likely due to Van der Waals forces and dehydration, which particularly affect smaller nanoparticles [68].

EDX and elemental mapping analysis

FE-SEM analysis of the tested sample displayed spherical nanoparticles with an average particle size range

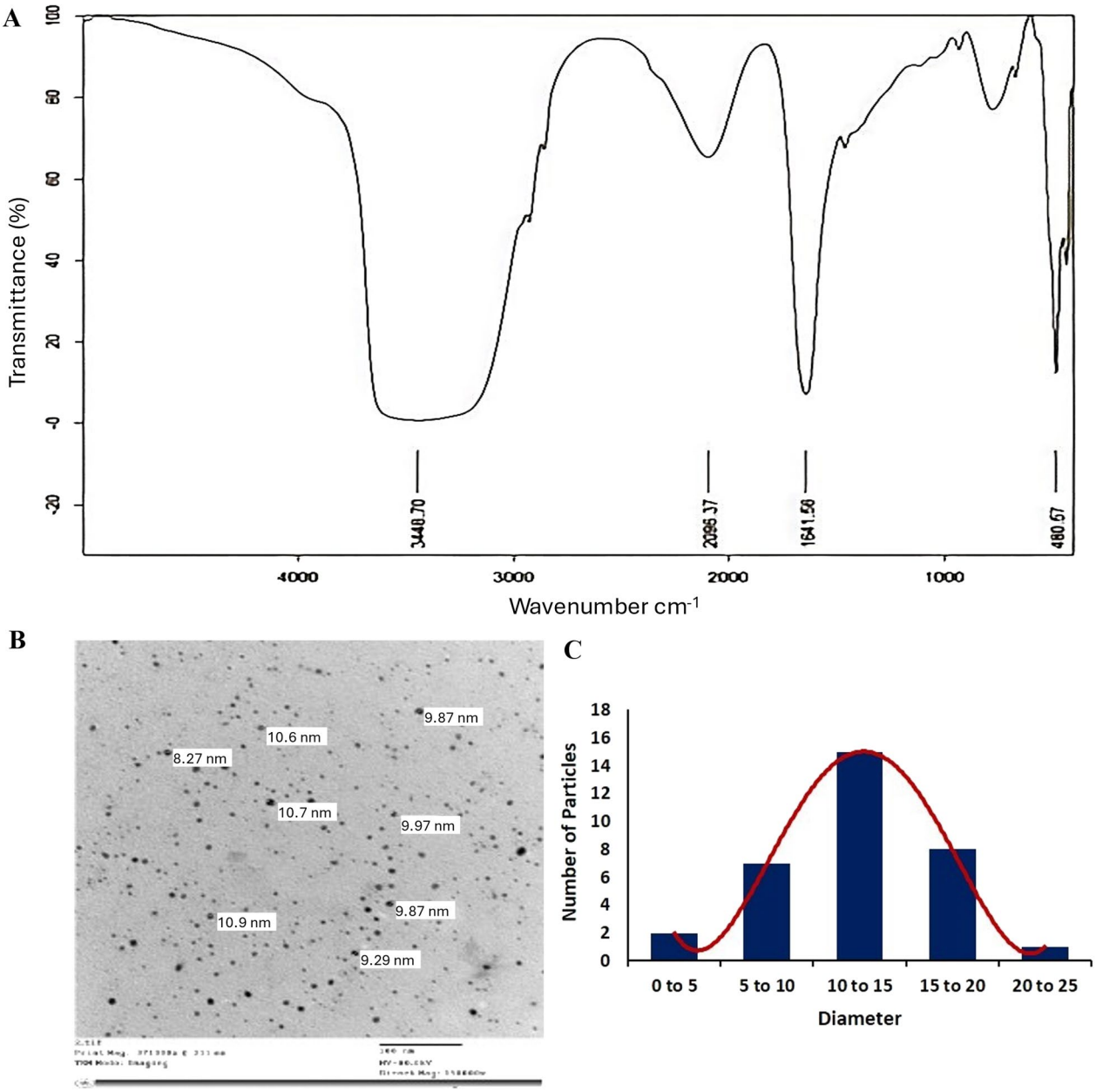

Fig. 6 FTIR spectrum (**A**), transmission electron image (**B**), and histogram of Bio-Ag_2ONPs of different sizes (**C**)

of 45.39 nm (Fig. 8A). In Fig. 8B, the EDX elemental mapping results confirm the Ag_2ONPs elemental composition, with a strong and sharp elemental signal peak at approximately 3 keV, characteristic of AgNPs absorption [69]. In addition, weaker carbon and oxygen atom signals were detected in the spectrum (yellow) (Fig. 8B).

The elemental mapping results of Ag_2ONPs, as presented in Fig. 8C, demonstrated that the selected scan area of the sample resembled that of silver (turquoise blue), with 64% Ag and 36% oxygen present in Fig. 8D. This observation suggests that silver and oxygen ions were predominant in the tested samples. The absence of any additional peaks or signals corresponding to other elemental components in the characterization data confirms the high purity of Bio-Ag_2ONPs, as revealed in Fig. 8E. This observation is harmonized with previous reports on the biosynthesis of AgNPs using *Tectona grandis* seed extract [70], where comparable results demonstrating the purity of the synthesized nanoparticles were

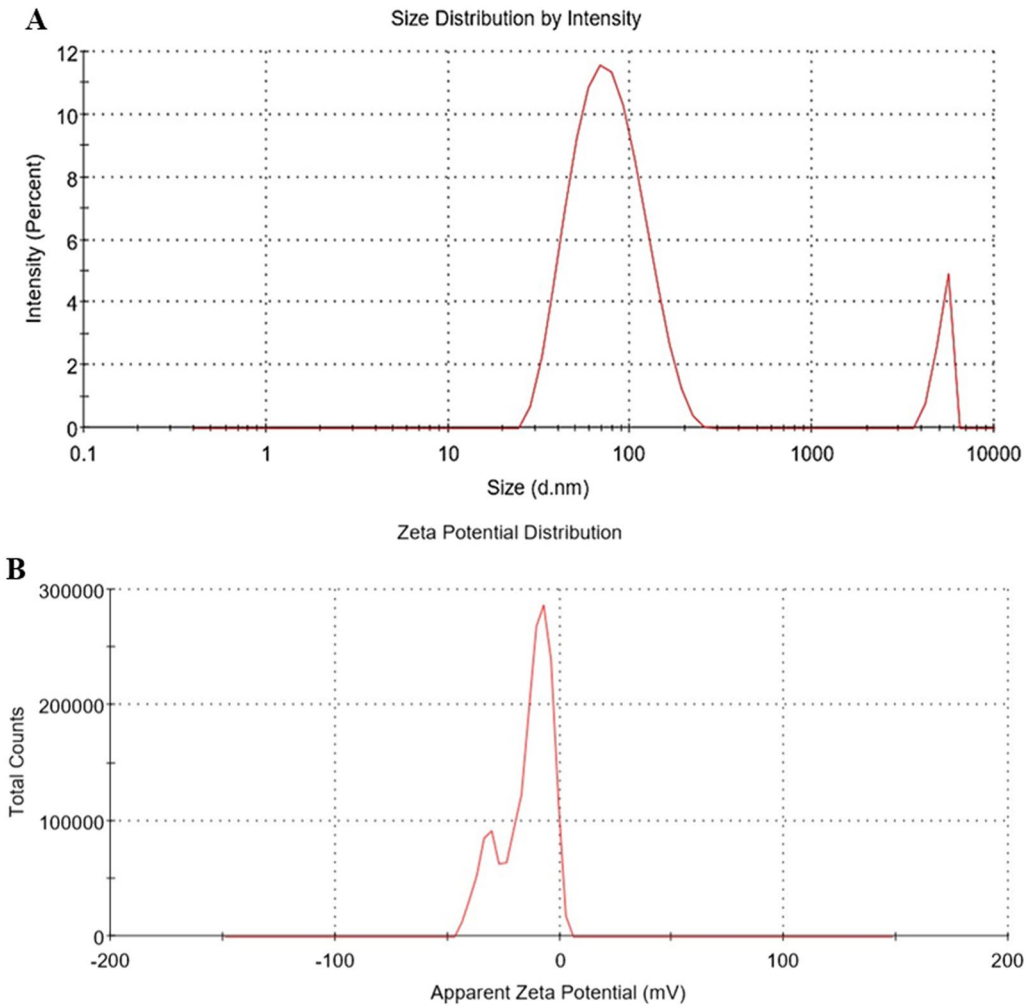

Fig. 7 DLS measurements of Bio-Ag_2ONPs size distribution (**A**) and zeta potential (**B**)

obtained. In the context of nanoparticle synthesis, purity is a crucial factor because the presence of impurities or other elements can significantly affect the properties and performance of the NPs. The absence of additional elements in the characterization results, such as in Fig. 8F, indicates that the synthesis method employed was effective in producing highly pure Ag_2ONPs without significant contamination or byproducts.

Previous studies [71, 72] have reported similar findings, wherein the characterization techniques employed confirmed the purity of the synthesized nanoparticles. These consistent observations across different research groups and synthesis methods reinforce the reliability and reproducibility of the results.

The apparent contradiction between FTIR and EDX can be explained by the fact that EDX primarily detects the elemental composition of the nanoparticles themselves, while FTIR is sensitive to the organic molecules or biomolecules present in the sample, which may be adsorbed or bound to the nanoparticle surface [73, 74].

It is important to note that the EDX analysis does not necessarily rule out the presence of organic compounds or biomolecules, as these typically contain lighter elements (e.g., carbon, hydrogen, nitrogen, oxygen) that are more challenging to detect using EDX, especially when present in trace amounts or as surface coatings.

X-ray diffraction analysis (XRD)

The XRD patterns of Ag_2ONPs showed peaks of 27.7, 32.16°, 46.12°, 46.36, 54.69, 57.32, 67.37°, and 76.63° which are indexed to 110, 111, 200, 211, 220, 221, 013 and 311, respectively (Fig. 9A). The resulting patterns showed sharp reflections corresponding to the face-centered cubic crystal configuration of Ag_2O [75]. The calculated average crystallite size of the biosynthesized Ag_2ONPs was 12.9 nm which was supported by the TEM calculations. By comparing the data with the diffraction pattern

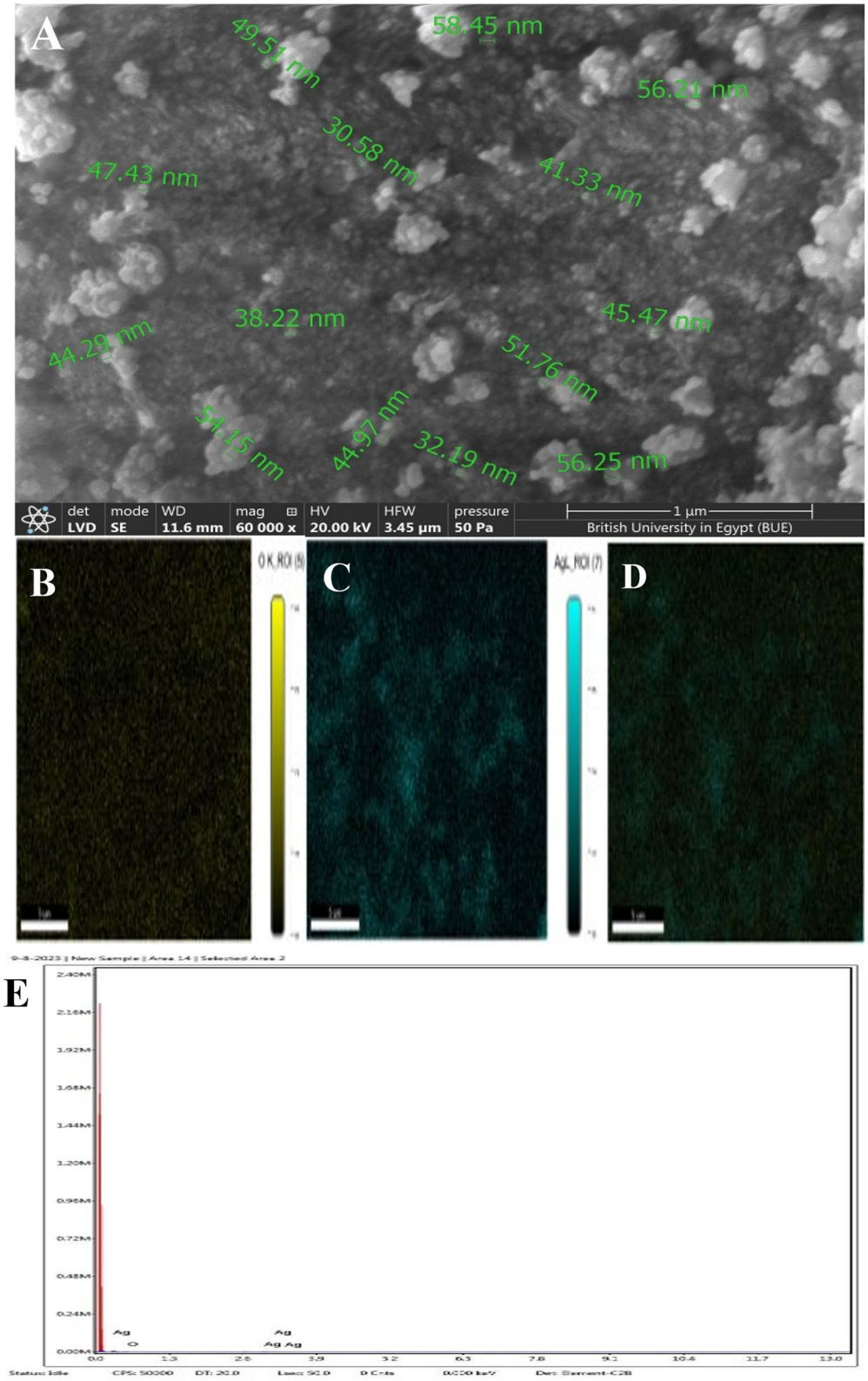

Fig. 8 SEM image of biosynthesized Ag_2O with dimention (**A**), energy dispersive spectroscopy (EDS) analysis, and elemental mapping of the silver oxide nanoparticle composition (**B**, **C**, and **D**) and elemental analysis spectrum (**E**)

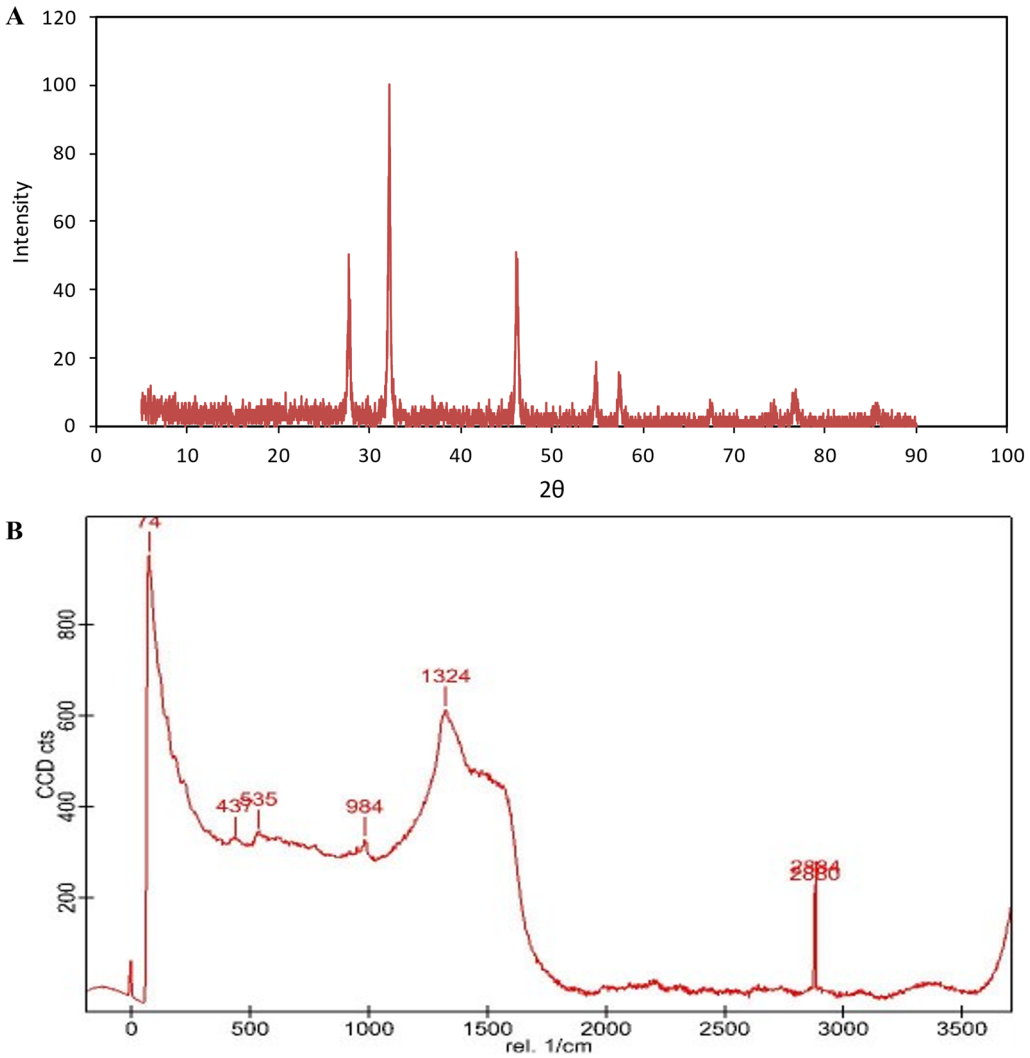

Fig. 9 XRD analysis (**A**) and Raman shift of Bio-Ag_2ONPs (**B**)

standard (JCPDS file No. 04–0783), the resulting patterns showed sharp reflections corresponding to the face-centered cubic crystal configuration (FCC) of Ag_2O [76]. The XRD outline of biosynthesized silver nanoparticles produced by *Bacillus cereus* sp. showed 4 peaks in the entire spectrum of 2θ values extending from 20 to 80 [44].

Raman analysis

The presence of Ag_2O was confirmed by Raman scattering (Fig. 9B). Seven distinct peaks were observed at wavenumbers of 74, 439, 535, 984, 1324, 2880, and 2884 cm^{-1}. The peak detected at 74 cm^{-1} suggests a low-frequency vibrational mode, potentially indicating lattice vibrations or structural distortions within the Ag_2O nanoparticles, providing insights into their stability and arrangement. The reported peaks at 439 and 535 cm^{-1} correspond to the vibrational modes associated with the stretching of the Ag–O bonds in Ag_2O NPs [77]. Notably, Harroun et al. observed bands near 490 cm^{-1} in the Raman spectrum of pure Ag_2O, which were attributed to simplification. The peaks at 984 and 1324 cm^{-1} may be referred to the presence of silver carbonate resulting from the interaction between the oxide and CO_2 [78, 79]. The presence of the carbonate band was most likely due to the extended duration of nanoparticle exposure to the atmosphere during the Raman data acquisition. Moreover, the peaks recorded at 2880 and 2884 cm^{-1} fell within the typical range of C–H stretching vibrations, which might indicate the presence of organic matter in the bacterial culture.

Table 3 Antibacterial activities of Bio-Ag_2ONPs against MDR wound pathogens

Bacterial strain	Inhibition zone diameter (mm)				
	Ag_2ONPs (μg mL^{-1})				
	100	50	40	30	20
EC–3	23 ± 0.17^{d}	22 ± 0.19^{cd}	21 ± 0.23^{c}	19 ± 0.42^{b}	17 ± 0.21^{a}
PA–09	14 ± 0.23^{d}	12 ± 0.15^{c}	11 ± 0.17^{bc}	10 ± 0.23^{b}	8 ± 0.17^{a}
KP–1	18 ± 0.26^{d}	16 ± 0.14^{c}	15 ± 0.16^{c}	10 ± 0.21^{b}	9 ± 0.14^{a}
SA–17	12 ± 0.14^{d}	10 ± 0.16^{c}	8 ± 0.19^{b}	6 ± 0.19^{a}	7 ± 0.16^{a}

Different superscript letters in each row reveal substantial differences at $p < 0.05$, as determined by Duncan's test. $AgNO_{3\ was}$ used as a -ve control and had no effect

Table 4 MIC, MBC and tolerance value of Bio–Ag_2ONPs against MDR wound pathogens

Microbial strain	MIC (μg mL^{-1})	MBC (μg mL^{-1})	Tolerance value (MBC/MIC)
EC–3	1.56	3.125	2
PA–09	6.25	12.5	2
KP–1	6.25	12.5	2
SA–17	25	100	4

Antibacterial activities of Bio-Ag_2ONPs

The antibacterial activities of the Bio-Ag_2ONPs were examined against four MDR wound pathogenic bacteria. As shown in Table 3, the effects of Bio-Ag_2ONPs on the examined strains varied slightly. Interestingly, EC-3 exhibited the highest susceptibility to Bio-Ag_2ONPs, followed by KP-1 and PA-09, while SA-17 displayed the least sensitivity. The observed antibacterial activity patterns are consistent with the findings reported by Panacek et al. [80], who noted that Gram-positive bacteria exhibited greater resistance to silver oxide nanoparticles (Ag_2ONPs) compared to Gram-negative bacteria.

This differential susceptibility could be partially attributed to the dense peptidoglycan layer present in the cell walls of Gram-positive bacteria, which may impede or limit the entry of nanoparticles into the cells [81].

The MIC of Bio-Ag_2ONPs against selected strains are shown in Table 4, ranging from 1.56 μg mL^{-1} to 25 μg mL^{-1}. A minimal MIC value was observed against EC-3 (1.56 μg mL^{-1}), whereas SA-17 was the least susceptible strain with the highest MIC value (25 μg mL^{-1}). The MICs observed in this study were notably lower than those documented for *S. aureus* and *E. coli* (62.5 μg mL^{-1} and 15.6 μg mL^{-1}, respectively) in a study by Bakhtiari-Sardari et al. [82]. The MBC values were twice the inhibitory concentrations against the tested strains, except for SA-17, which exhibited an MBC value of 100 μg mL^{-1}. The MIC of Bio-Ag_2ONPs bacterial strains was significantly lower compared to the findings reported by Singh et al. [83] In their study, Singh et al. examined the MIC of biogenic silver nanoparticles (AgNPs) against various bacteria. For a range of Gram-negative bacteria, including *Escherichia coli*, *Acinetobacter baumannii*, *Enterobacter aerogenes*, *Pseudomonas aeruginosa*, *Salmonella typhimurium, and Shigella sonneii*, they found MIC values ranging from 150 to 600 μg mL^{-1}. In contrast, for Gram-positive bacteria such as *Staphylococcus aureus* and *Streptococcus mutans*, the MIC values exceeded 1000 μg mL^{-1}.

This comparison highlights that the Bio-Ag_2ONPs in the current study demonstrated higher antimicrobial efficacy, requiring lower concentrations to inhibit bacterial growth compared to the biogenic AgNPs examined in Singh et al.'s research. It also reinforces the observation that Gram-negative bacteria are generally more susceptible to silver nanoparticles than Gram-positive bacteria, as evidenced by the lower MIC values for Gram-negative species in both studies.

AgNPs are known for their potent antimicrobial activity, and several factors influence their bactericidal mechanisms, such as concentration, bacterial class [84], shape [85], and size [86]. In our study, the strong antimicrobial effect of Ag_2O NPs at relatively low concentrations could be attributed to their smaller size, which allows them to easily diffuse across the cell wall and penetrate cells, releasing silver ions faster compared to larger particles. Additionally, the spherical shape of the NPs allows them to interact with pathogens with the largest surface area available.

Various modes of action have been proposed. Small size and spherical biosynthesized Ag_2O NPS could simply enter the cell walls [87] and interact with cellular structures and different biochemicals such as DNA, protein molecules and lipids. Thus, causing structural damage, cell wall rupture, and leakage of intracellular components [87]. Smaller NPs could also adhere to cell membranes interfere with lipids, LPS, and proteins and induce more reactive oxygen species (ROS) [46]. ROS are solid oxidizing agents that oxidize lipids and proteins in the cell and cause DNA damage. Silver ions interfere with cellular processes by attaching to enzyme proteins and DNA, hampering cell division. Among various nanomaterials, silver nanoparticles show the highest stability in thermal and aqueous environments. They demonstrate potent antifungal effects against multiple *Candida* species at a minimum inhibitory concentration of 50 μg mL^{-1} [46]. The antimicrobial action of silver oxide nanoparticles (Ag_2O NP) involves a specific mechanism. These nanoparticles emit silver ions (Ag^{+}) upon nearing bacterial cells. The ions then interact with sulfur and

phosphorus-containing molecules in the bacterial cell wall, leading to structural disruption and the creation of small cavities [88].

These pits compromise the cell wall's integrity, allowing the entrance of ions and other foreign substances into the cell. This influx leads to an increase in intracellular osmotic pressure, causing the cell to swell. Eventually, the accumulating pressure results in the rupture of the cell wall and subsequent cell lysis.

The antimicrobial action of silver nanoparticles is notably more effective against Gram-negative bacteria compared to Gram-positive bacteria. This difference in susceptibility is attributed to variations in cell wall composition. Gram-positive bacteria possess a thicker, more extensively cross-linked peptidoglycan layer and contain teichoic acid in their cell walls, providing greater protection. In contrast, Gram-negative bacteria have a thinner or absent peptidoglycan layer and a higher proportion of lipopolysaccharides in their cell walls. This structural difference makes Gram-negative bacteria more vulnerable to silver nanoparticle interactions due to reduced cellular barriers [89].

Time-kill curve

The bactericidal properties of Bio-Ag_2ONPs on the tested strains over time were analyzed. As seen in Fig. 10 A, B, C, and D, a reduction in the rate of growth was detected in the tested bacteria with increasing time compared to the control; complete inhibition of EC-3 cells was observed after 6 h. Additionally, a total reduction occurred after 8 h for the other tested strains. The results showed that Ag_2ONPs had a variety of kinetics against the pathogens that were tested, and they successfully stopped their growth at a low concentration of Ag_2ONPs. This variability in response may be referred to the different Ag_2ONPs' modes of action and bacterial cell metabolism or structure.

Transmitted electron microscope

The antibacterial activity of Bio-Ag_2ONPs against *E. coli* EC-3, the most susceptible strain was investigated using TEM imaging. Untreated bacteria displayed a uniform nuclear area and well-dispersed cytoplasm, with intact, well-defined, rod-shaped cells (Fig. 11A). However, upon treatment with Bio-Ag_2ONPs, significant changes in bacterial shape were observed, along with cell rupture and discharge of cytoplasmic material (Fig. 11B).

The antimicrobial of Bio-Ag_2ONPs might be due to the various proposed modes of action. For example, small and spherical Bio-Ag_2ONPs can easily penetrate the cell walls, react with protein molecules on the cell surface, and cause structural damage, cell wall rupture, and leakage of intracellular components (Fig. 10B). Moreover, nanoparticles can adhere to cell membranes, stimulate the generation of reactive oxygen species, and consequently trigger DNA damage and cell death. Additionally,

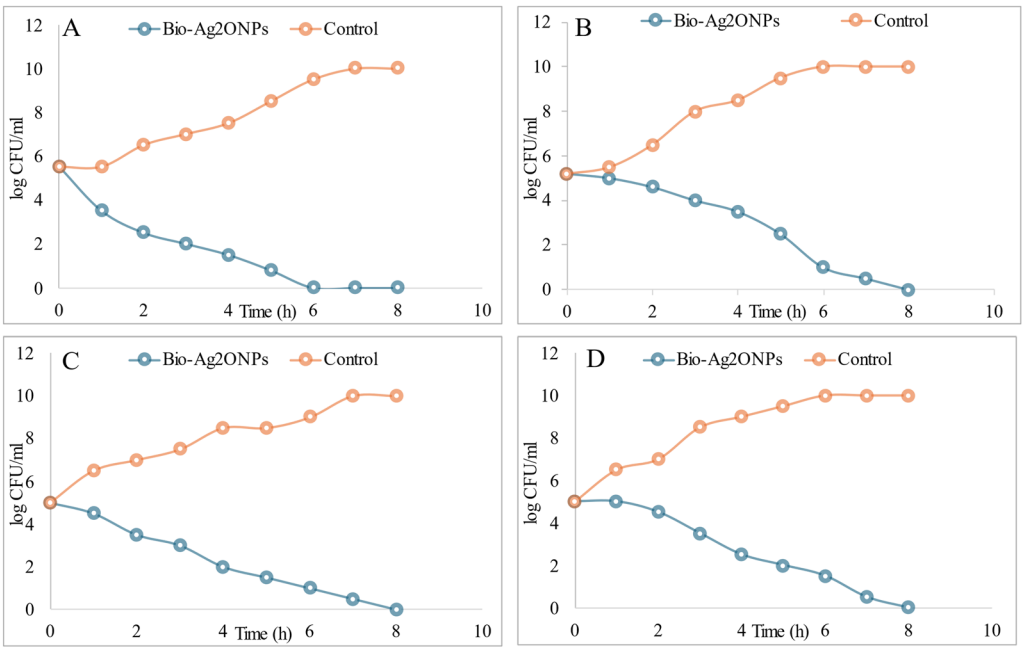

Fig. 10 Time-kill curves of the examined MDR pathogenic bacteria: **A** *E. coli* (EC-3), **B** *P. aeruginosa* (PA-09), **C** *K. pneumoniae* (KP-1), and **D** *S. aureus* (SA-17). The values correspond to the mean ± SD of three distinct observations

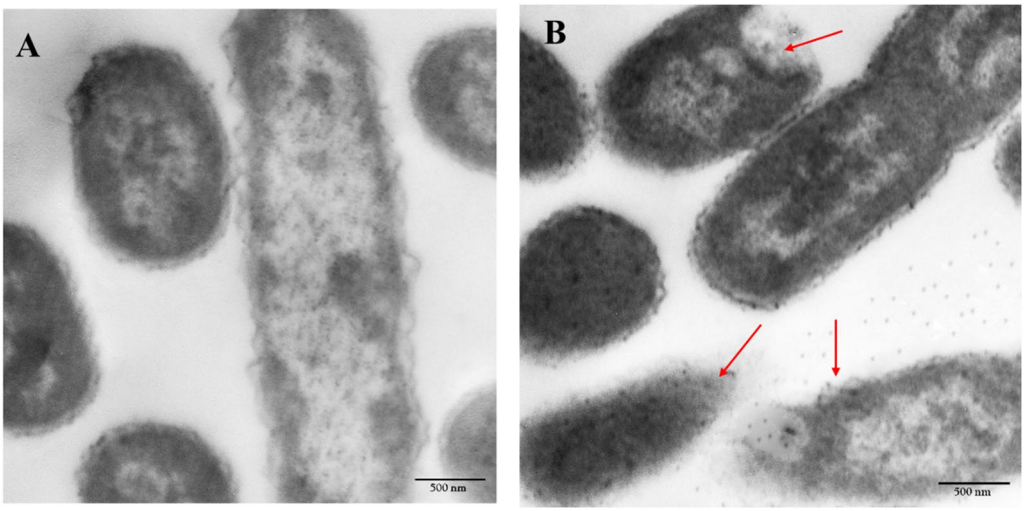

Fig. 11 TEM images of *E. coli* EC-3 strain (5000X). Untreated cells with intact cell membranes (**A**). Cells treated with Bio-Ag_2ONPs resulted in morphological changes in the bacteria and lysis of cells (arrows) (**B**)

silver ions readily bind to enzyme proteins containing sulfhydryl (–SH) groups, thereby deactivating essential enzymes and impeding cell divisio. Moreover, the interaction of Ag^+ with DNA bases can disrupt the natural architecture of DNA and influence cell division. Nanoparticles tend to target the respiratory chain and impede cell division, ultimately resulting in cell death [90–92]. the Ag_2ONPs tolerance level for each strain was determined using the respective MIC and MBC values. Therefore, the tolerance level was 2 for strains EC-3, PA-09, and KP-1, whereas strain SA-17 displayed a tolerance level of 4. The MBC/MIC ratio, which reflects the tolerance level, served as a parameter that demonstrated the bactericidal ability of the tested compound. If the MBC/MIC ratio is ≤ 4, the antimicrobial agent is bactericidal [93]. Thus, Bio-Ag_2ONPs possess potent bactericidal activity against the tested strains.

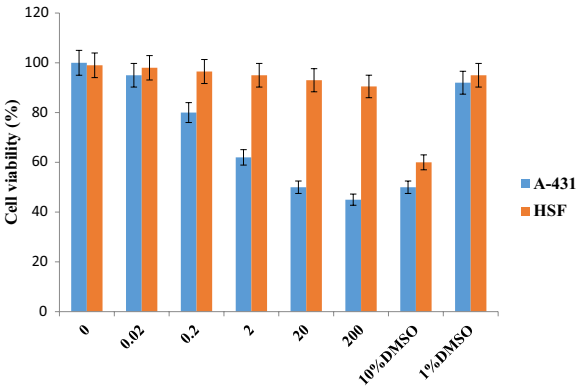

Fig. 12 Cytotoxic effects on A-431 and HSF cells exposed to various concentration of Ag_2ONPs and DMSO for 48 h

Cytotoxicity assay

Assessment of cytotoxicity plays a crucial role in developing safe and efficient medications [94, 95]. In our investigation, we used two in vitro models, A-431 and HSF cell lines, to assess the cytotoxic effects of Bio-Ag_2ONPs. Cytotoxicity was evaluated using an SRB assay. As illustrated in Fig. 12, the cytotoxic properties of Bio-Ag_2ONPs on both malignant and normal cell types. The findings indicated that Ag_2ONPs exhibited no toxicity towards the HSF cell line, allowing for regular cell metabolism and development (IC_{50} greater than 200 µg mL^{-1}). The results confirmed that Bio-Ag_2ONPs exhibited excellent biocompatibility and safety towards normal cells, demonstrating no cytotoxic effects on the normal cell line tested. This suggests Bio-Ag_2ONPs could potentially be used as a biocompatible agent or material.

In contrast, the Bio-Ag_2ONPs displayed the ability to decrease the viability and proliferation of cancer cells in a dose-based mode, as illustrated in Fig. 12. Higher concentrations or doses of the Bio-Ag_2ONPs led to greater reductions in cancer cell viability. Increasing the exposure duration resulted in increased cytotoxicity in the cells. A-431 cells were significantly less likely to live when Bio-Ag_2ONPs were added at a dilution of 2 µg mL^{-1} or higher. The half-maximal inhibitory concentration (IC_{50}) of Bio-Ag_2ONPs was detected to be 20 µg mL^{-1} for A-431 cells. Significantly, the analysis of IC_{50} data suggested that Bio-Ag_2ONPs had greater cytotoxicity against tumor cells compared to a normal cell line. Consequently, Ag_2O NPS have the potential to be used as natural antitumor agents with no side effects. Analogous findings

were found by El-Zawawy et al. [33] on the HSF cell line, whereby they found that myco-silver nanoparticles, as a harmless chemical, enhance cell survival. In addition, Firdhouse et al. [2023] showed that bio-AgNPs are an influential anticancer treatment against the MCF-7 cell line.

Assessment of apoptosis by flow cytometer

Apoptosis, also known as programmed cell death, is a hallmark of cancer treatment [96]. Therefore, tumor cytotoxicity and apoptosis induction could be the preferred methods for the treatment of various cancer types. Hence, annexin V and PI staining are commonly used as quantitative and qualitative approaches to evaluate apoptosis. The flow cytometry findings for A-431 cells administered 20 µg mL^{-1} of Bio-Ag_2ONPs for 48 h and compared to the control are shown in Fig. 13A and B. A significant induction of early apoptosis was observed in 13% of the treated cells (Fig. 13B) compared to 0.84% of the control (Fig. 13A). However, the number of cells undergoing late apoptosis due to Bio-Ag_2ONPs was significantly higher (38.68%) than that in the control cells (2.19%). The percentages of cell viability, early and late apoptosis, and cell death are shown in Fig. 13C. Multiple investigations have shown that these nanoparticles can control many cellular processes, including DNA repair, the cell cycle, apoptosis, and various cell signaling cascades [97–99]. A plethora of studies have recently

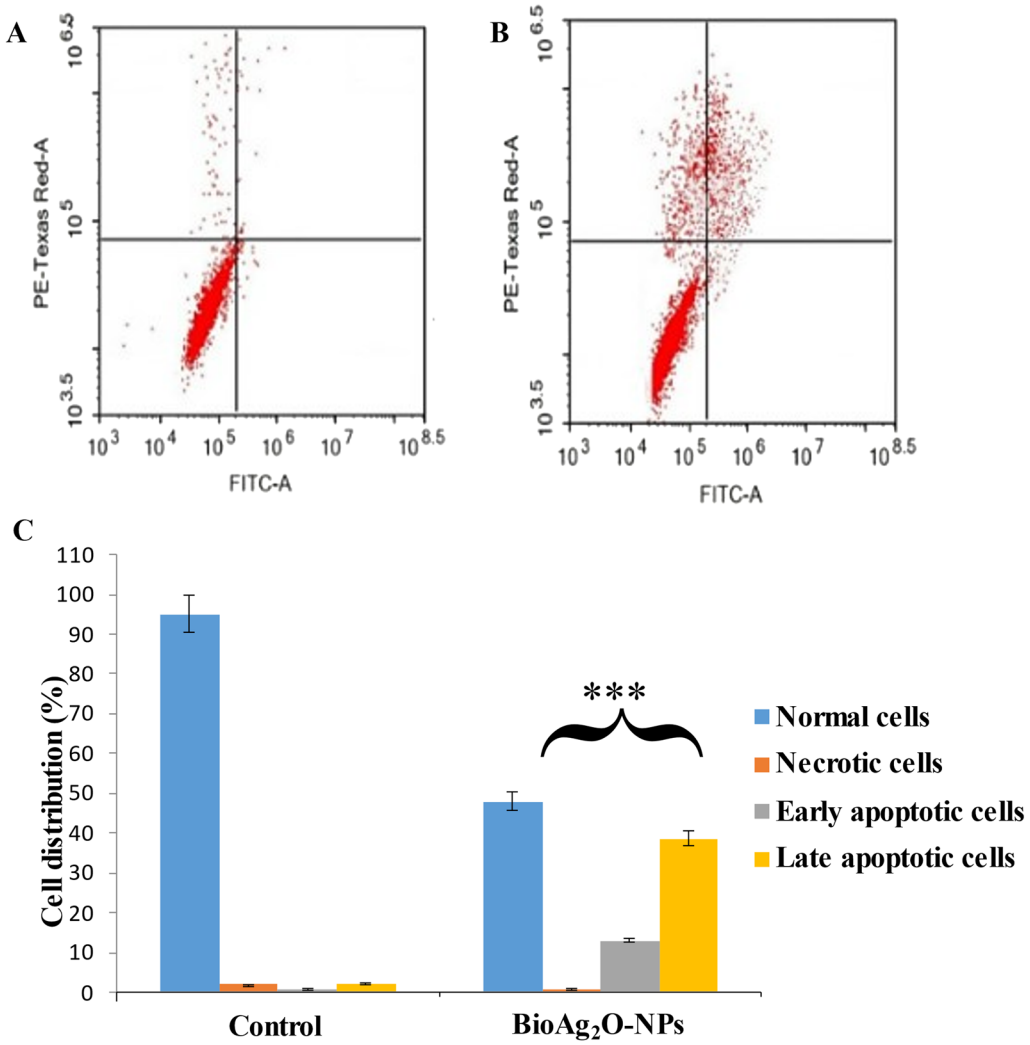

Fig. 13 Bio-Ag_2ONPs prompt apoptosis in A-431 cells. The alteration in apoptotic cells within A-431 cell lines exposed to the IC50 concentration of Bio-Ag_2ONPs for 48 h (**A**; control without treatment and **B**; treated cells) and quantification of necrotic, normal, early and late apoptotic cells in both treatments (**C**). Data are presented as mean ± SD from three distinct experiments. ***P < 0.001, indicating statistical significance

highlighted the benefit of nanoparticles as potential therapeutic means against cancer. However, to the best of our knowledge, the impact of Bio-Ag_2ONPs on A-431 is largely unexplored. Thus, in this study, we assessed the anticancer potential of Bio-Ag_2ONPs against A-431.

Real-time PCR (qRT-PCR)

Dysregulated pathways associated with uncontrolled cell proliferation and apoptosis evasion, hallmarks of cancer, and treatment resistance were targeted in our study [100, 101]. Real-time PCR (qRT-PCR) was employed to investigate the induction of apoptosis in A-431 cells following a 24 h incubation with Bio-Ag_2ONPs. The expression levels of several apoptotic genes including Bcl-2 associated X protein (*Bax*), B-cell lymphoma 2 (Bcl-2), Caspase-3 (*Cas-3*), and guardian of the genome (*P53*) were evaluated. *Bax* and *P53* promote apoptosis, Bcl-2 inhibits it, and Caspase-3 carries out the final demolition of the cell during the apoptotic process [102]. The balance between these pro- and anti-apoptotic genes helps determine whether a cell will live or die at any given time. Upon treatment with 20 µg mL^{-1} Bio-Ag_2ONPs, a substantial reduction in the mRNA level of Bcl-2 was recorded in A-431 cells (Fig. 14). Conversely, the mRNA expression levels of *Cas-3*, *Bax*, and *P53* exhibited a notable increase after 24 h. Specifically, the pro-apoptotic *Bax* gene was upregulated, while the anti-apoptotic Bcl-2 gene was downregulated in cancer cells treated with 20 µg mL^{-1} Bio-Ag_2ONPs for 24 h. Additionally, exposure to Bio-Ag_2ONPs resulted in elevated expression levels of *P53* and Casp-3 genes in A-431 cells. These proteins play crucial roles in cell cycle arrest, cancer suppression, and the apoptosis-killing phase [103, 104]. Our findings suggest that increased levels of Bio-Ag_2ONPs may alter the genes expression involved in cell death, mitochondrial membrane potential loss, and apoptosis. Similar correlations have been reported in other researchers [59, 105, 106]. Consistent with our results, previous studies have demonstrated that cancer cells treated with AgNPs exhibit enhanced expression of the pro-apoptotic *Bax* protein [107–109], indicating the potential efficacy of Bio-Ag_2O-NPs as an agent against cancer cells.

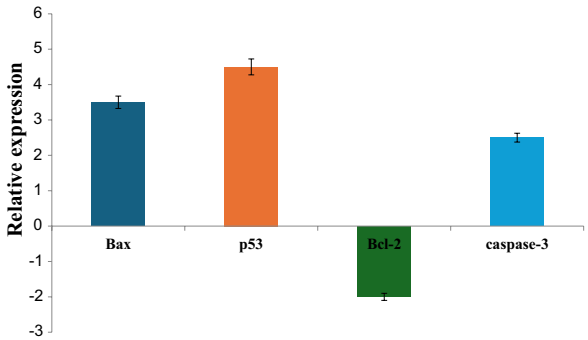

Fig. 14 Expression levels of the examined genes (*Bax*, *P53*, Bcl-2, and *Cas-3*) in A-431 cells following treatment with the IC50 of Bio-Ag_2O NPs. All transcripts were normalized to the reference gene (18S RNA). All data are presented as fold-change in A-431 cells after treatment with Ag_2O NPs compared to untreated A-431 cells, where the expression levels of the genes were set as 1

Materials and methods

Materials

Silver nitrate was purchased from Sigma-Aldrich (St. Louis, MO, USA). Louis, Mo. (USA) and trichloroacetic acid (TCA) was obtained from Merck (Germany). All microbial culture media (Luria–Bertani (LB), Mueller Hinton broth (MHB), trypticase soy broth (TSB), and nutrient agar media) were sourced from Hi Media Laboratories Pvt. Ltd., Mumbai, India.

Plant material and isolation of endophytic bacteria

Healthy leaves of *Lycium shawii* Roem & Schult were randomly collected and cleaned thoroughly with streaming tap water to remove aatached soil particles adhereing to the surface. The leaves were then rinsed with distilled water. Treatment with 0.1% v/v Tween 20 detergent was performed, ensuring complete coverage of the sample, and rinsing continued until the washing water became clear. Surface sterilization was then conducted to remove epiphytic microorganisms by dipping the leaves in 4% sodium hypochlorite for 5–10 min, followed by 2.5% v/v $Na_2S_2O_3$ for 10 min, and finally dipping in 70% ethanol for 2 min [110]. The sterilized leaves were subsequently washed four to six times with sterilized distilled water to remove any residual chemicals. A final rinse with $NaHCO_3$ (10% v/v) was performed for 10 min to remove any traces of the previously used chemicals.

Under aseptic conditions, the disinfected leaves, with the midribs removed, were pulverized in a sterile mortar using 6 ml of sterile aqueous saline solution (0.9% NaCl). A sterile aqueous solution was used to serially dilute the tissue extract. Approximately 100 µL of each diluted sample (10^{-1} and 10^{-2}) and undiluted sample were equally distributed onto Luria–Bertani agar plates (supplied with fluconazole (100 mg L^{-1}) to prevent endophytic fungal growth) using a sterilized glass spreader. Petri dishes were incubated at 30 ± 2 °C and deceted at regular intervals for bacterial growth (1–3 days). After incubation, eight endophytic bacterial isolates were obtained and subjected to multiple rounds of purification using the streaking method on fresh LB agar plates. These plates were then incubated for 2 days and checked for culture purity. Eventually, the pure cultures were transferred to LB agar slant tubes for further use. Glycerol stocks (10%

v/v) were maintained and stored at − 80 °C for long-term preservation.

Screening of silver nitrate reducing endophytic bacteria

Endophytic bacterial isolates were screened for silver nitrate reduction as described by Ameen et al. [111]. This involved subculturing on LB agar plate medium (5 g yeast extract, 10 g tryptone, 20 g agar, and 1 L dist H_2O, pH 7.5 ± 0.1, without NaCl) supplemented with 0.5 mM filter-sterilized $AgNO_3$ solution and incubated at 30 °C for 48 h in dark conditions and observe the bacterial growth to assess their ability to reduce silver nitrate. Colonies that have a brown color were evaluated as silver nitrate-reducing strains. After screening, only one strain, AUMC-B 524, a silver nitrate reducer,, was selected for further investigation. Subsequently, strain AUMC-B524 was maintained on slant agar supplemented with 0.1 mM silver nitrate at 4 °C for subsequent studies.

Molecular identification of Ag_2ONP-producing endophytic bacteria

The selected endophytic bacterium was identified at the molecular level according to El-Sapagh et al. [112]. The endophytic bacteria was cultivated in LB broth medium at 37 °C for 24 h. The Patho Gene-Spin DNA/RNA extraction kit, supplied by Intron Biotechnology, was utilized to extract and purify genomic DNA. PCR was used to amplify the 16S rRNA gene. The purity of PCR products (amplicons) was validated by electrophoresis on a 1% agarose gel using a small nucleotide marker (100 base pairs). The amplicons that had been purified were subjected to sequencing in both the sense and antisense directions. This was achieved by utilizing 27F and 1492R primers when di-deoxynucleotides (dd NTPs) were added to the reaction mixture [113].

Biosynthesis of Bio-Ag_2ONPs

For the biosynthesis of Bio-Ag_2ONPs, the selected endophytic bacterial strain was freshly inoculated in a sterile LB broth medium free from NaCl (pH 7.5 ± 0.2) and incubated in a rotating shaker (140 rpm) for 24 h at 37 ± 2 °C. Following the incubation period, the bacterial cultures underwent centrifugation for 20 min at 6000 rpm to collect the supernatant required to synthesize Ag_2ONPs. In this experiment, one mM filter-sterilized silver nitrate aqueous solution was mixed separately with the collected supernatant in equal volumes. All the reactions were shacked (200 rpm) on an orbital shaker at 30 ± 2 °C for a duration of 48 h in dark conditions to reduce the photoactivation of $AgNO_3$. Control was conducted using uninoculated media and $AgNO_3$ solution to investigate the influence of bacteria on nanoparticle synthesis. Preliminary detection of the biosynthesized Ag_2ONPs was monitored through the visual color change from watery yellow to reddish brown at the end of the incubation period due to the reduction of $AgNO_3$ and formation of Ag_2ONPs [114]. The amount of reduction was estimated spectrophotometrically at 200–800 nm using UV–vis spectrophotometer (Dual Beam Spectrophotometer, UV-1800, Shimadzu, Kyoto, Japan) [115].

Experimental designs for optimizing Ag_2ONPs

Screening vital variables for Ag_2ONPs biosynthesis using Plackett–Burman design (PBD)

Biosynthesis optimization for maximal Ag_2ONPs production was conducted by a statistical approach using the Plackett–Burman design (PBD) to select factors that significantly influenced the production of silver oxide nanoparticles [116]. The Design-Expert 7.0 statistical software was used for this analysis (Stat Ease Inc., Minneapolis, U.S.A). In this investigation, six independent variables were considered to represent the biosynthesis conditions, including bacterial supernatant concentration, $AgNO_3$ concentration, pH, temperature, reaction time, and illumination (Table S3). The biosynthesis of Ag_2ONPs was determined through spectrophotometric analysis of the resulting solutions' absorbance at 422 nm. All experiments were conducted 3 times, and the average of Bio-Ag_2ONPs was detected as the response. Fisher's test for analysis of variance (ANOVA) was conducted to ascertain the statistical significance of the first-order model [117]. The experimental design employed by Plackett–Burman is founded upon the first-order model:

$$Y = \beta_0 + \sum \beta_i X_i \quad (2)$$

In this context, ″Y″ represents the predicted response or dependent variable, which is the biosynthesized Ag_2ONPs- the variable needed to be predicted. ″β_0″ denotes the model intercept, while ″β_i″ represents the linear coefficient. ″X_i″ indicates the level of an independent parameter, which help in explaining the production of Ag_2ONPs. The statistical significance of the variables was determined by estimating the t value, P value, and confidence level [118]. Variables that were determined to have a significant influence at a 95% level ($P < 0.05$) were included in the analysis [119].

Response surface optimization of Ag_2ONPs using box behnken design (BBD)

In order to improve Ag_2ONPs production, BBD was used to select three key factors that had a favorable impact on production. These factors were further optimized using RSM with a BBD [120]. The relationship between the major variables was determined using the response surface and contour plots of the model's expected responses.

The tries, regression, and graphical analysis of the data were conducted using Design-Expert version 8.0 (Stat-Ease Inc., Minneapolis, MN, USA).

These variables—bacterial supernatant concentration, $AgNO_3$ concentration, and pH—were coded as A, B, and C, respectively. Each factor was measured at three levels (−1, 0, +1), reflecting low, intermediate, and high values (Table S4). The design consisted of 17 experimental trials, each including distinct combinations of A, B, and C to ensure method repeatability. Triplicate experiments were conducted, with mean Ag_2ONPs yield as the response variable. Data was fitted using a second-order polynomial equation:

$$Y = \beta_0 - \sum \beta_i X_i + \sum \beta_{ij} X_i X_j + \sum \beta_{ii} {X_i}^2 \quad (3)$$

Here, ″Y″ represents the predicted response, ″β_0″ is the intercept, ″β_i″ denotes the linear coefficient, ″β_{ij}″ represents the interaction coefficient, ″β_{ii}″ signifies the quadratic coefficient, and ″X_i″ denotes the independent variables [121]. The fitted polynomial equation was depicted via three-dimensional surface graphics. Variable levels were optimized using Design-Expert's numerical optimization method to maximize the response.

Characterization of Bio-Ag_2ONPs

Fourier transform infrared (FTIR) spectroscopy

The FTIR spectroscopy analysis was performed using an IR spectrophotometer (Perkin-Elmer 1430, USA) equipped with an IR Affinity-1 model. The spectrophotometer features a wavelength range of 400–4000 cm $^{-1}$ and a resolution of 4 cm $^{-1}$ [122]. Prior to analysis, the powdered Ag_2ONPs were thoroughly dried and then combined with KBr to form pellets for analysis. FTIR spectroscopy is a powerful technique employed to analyze the intensity of infrared radiation at specific wavelengths, providing valuable insights into the potential interactions between functional groups involved in the reduction process.

Transmission electron microscopy (TEM)

The morphological characteristics of Bio-Ag_2ONPs were detected by TEM, according to Zhang et al. [123]. Thin films of Bio-Ag_2ONPs were prepared by depositing a small amount of the nanoparticle suspension onto a carbon-coated copper grid. The samples were then dried using a vacuum desiccator and visualized under a TEM microscope (JEOL JEM 1400, Japan).

Dynamic light scattering and zeta analyses

The average hydrodynamic size and surface charge of the Bio-Ag_2ONPs in an aqueous solution were estimated using dynamic light scattering (DLS). To achieve a homogeneous dispersion of nanoparticles, the NPs sample (1 mg mL^{-1}) was diluted 100 X in Milli-Q water (10 µg mL^{-1}) and subjected to ultrasonic processing. The resulting diluted working solution was subsequently analyzed using a Nano-Zeta Sizer-HT instrument (Malvern PANalytical, Malvern, Canada) [124, 125].

Energy dispersive X-ray (EDX) analysis

To characterize the size, shape, and elemental composition of Bio-Ag_2ONPs, field emission scanning electron microscopy (FESEM) (Quattro S, Thermo Scientific) coupled with energy-dispersive X-ray spectroscopy (EDX) analysis was employed. A (Quattro S, Thermo Scientific) solution of Bio-Ag_2ONPs was deposited onto a carbon-coated copper grid (300 µm mesh size), dried at 25 ± 2 ℃, and examined using a FESEM operating at 20 kV [126, 127].

X-ray diffraction (XRD) analysis

The crystallized form of the dried Bio-Ag_2ONPs was examined using X-ray diffractometer (Malvern Panalytical, Empyrean 3, Netherlands) equipped with Cu-Kα1 radiation (λ = 1.5406 Å wavelength). The sample underwent scanning over a 2θ range of 10°–90° at a scanning rate of 4° min^{-1} with a step size of 0.02°. Further analysis were carried out to identify the position, intensity, and width of the peaks. To determine the nanoparticle size, we used the the Debye–Scherrer equation:

$$D = \frac{K\lambda}{\beta \cdot \cos\theta} \quad (4)$$

where "D" is the average crystallite size, "K" is a geometric factor = 0.94, "λ" is the wavelength of the X-radiation (nm), "β" is the full width at half maximum (FWHM) of the XRD peak (in radians), and "θ" is the Bragg angle.

Confocal Raman microscopy

For Raman measurements, equal volumes (10 mL) of Bio-Ag_2ONPs suspension and double distilled water were mixed and sonicated for 20 min. A single drop of the suspension was dispensed onto a 0.2 mm-thick glass slide and covered for 48 h at 25 ± 2 °C. Following this incubation period, the samples were analyzed using a LabRAM HR Evolution Confocal Raman Microscope (Horiba Instruments, Kyoto, Japan). The optical microscope was outfitted with a 100 × objective lens with a numerical aperture (NA) of 0.90 and was connected to a Raman spectrometer (WITec alpha 300) [128]. All experiments of Bio-Ag_2ONPs characterization were carried out at Nanogate Inc. (Mokatam, Cairo, Egypt).

Antimicrobial assay

In this study, the Agar well diffusion method [129, 130] was utilized to estimate the Bio-Ag_2ONPs antimicrobial activities against four MDR wound pathogens obtained from our previous studies [131]. These strains are *Escherichia coli* EC-3, *Staphylococcus aureus* SA-17, *Klebsiella pneumonia* KP-1 and *Pseudomonas aeruginosa* PA-09. Pure cultures of the bacterial strains were cultured in MHB and incubated at 37 °C on a rotary shaker at 180 rpm. After incubation, cultures were adjusted to 10^7 CFU mL^{-1} using sterile saline solution. Sterile cotton swabs were used to equally distribute 100 µL of bacterial suspension from each tested strain onto separate sterile Mueller–Hinton agar plates.

Five wells were made on each inoculated agar plate using a sterilized 6-mm cork borer, positioned equidistantly. Each well was loaded with 100 µl of Bio-Ag_2ONPs at different concentrations (10–50 µg mL^{-1}). Next, the plates were incubated at 37 °C for 24 h, and measurements were taken to calculate the average of diameter of the inhibition zones surrounding each well.

The minimum inhibitory concentration (MIC) and minimum bactericidal concentration (MBC) were determined using the 96-well microtitre plate method, as previously described [132, 133]. Sterile saline solution were used to adjuste the microbial suspensions to the targeted concentration (1×10^6 CFU mL^{-1}). To achieve concentrations within the range of 1.56–100 µL mL^{-1}, the Bio-Ag_2ONPs were dissolved in LB broth medium (100 µL) along with the microbial inoculum per well. The microplates were then incubated for 24 h. Subsequently, the density was measured at 655 nm and compared to both negative and positive controls. Commercial antibacterial drugs such as streptomycin and ampicillin were utilized as positive controls [134]. To determine the MBC, 10 µL was obtained from each well that exhibited no visible growth after incubation. The sample was then spread onto Mueller–Hinton-Agar (MHA) plates for further incubation. After 24 h, the plates were visually examined, and the MBC, which represents the minimum concentration of Ag_2ONPs that completely prevented the proliferation of microorganisms on agar media, was documented. All of the assays were performed in triplicate.

The tolerance levels of the tested strain against Bio-Ag_2ONPs were estimated according to the technique of May et al. [135] using the following formula:

$$\text{Tolerance} = \text{MBC}/\text{MIC} \tag{5}$$

Additionally, the impact of Bio-Ag_2ONPs on bacterial morphology was visualized via transmission electron microscopy (TEM) (JEOL-JEM-100SX, Japan).

Time-kill assay

This assay was conducted following a previously described procedures of Guggenbichler et al. [136] and Zainin et al. [137], with some modifications. Initially, the bacterial cells were grown in the MHB and incubated at 37 °C with agitation at 121 rpm. The tested strains were grown until reaching an OD_{595} of 0.5, and then the cell concentration was adjusted to 10^6 CFU mL^{-1}. Then, the culture tubes were treated with Bio-Ag_2ONPs (at their respective MBC values) and incubated at 37 °C with 121 rpm agitation. Samples were collected at the desired time points (0–10 h) and inoculated on MHA plates. After incubating, the number of viable colonies was recorded by plate counts and quantified in CFU mL^{-1} [138]. The cultures that were not exposed to Ag_2ONPs were taken as controls, and the experiments were repeated three times.

Cytotoxic activity of Bio-Ag_2ONPs

Cell culture

The anticancer efficacy of the Bio-Ag_2ONPs was evaluated using two different cell lines—a normal human skin fibroblast (HSF) cell line and a human epidermoid skin cancer cell line (A-431). Both cell lines were obtained from Nawah Scientific Inc. (Cairo, Egypt). All cells were cultivated using Dulbecco's Modified Eagle Medium (DMEM) that was supplemented with 10% heat-inactivated fetal bovine serum, and 100 mg mL^{-1} penicillin and 100 units mL^{-1} streptomycin. The cell culture conditions involved incubating the cells at 37 °C in a moistened atmosphere containing 5% (v/v) CO_2.

Sulforhodamine B (SRB) assay

Cell viability experiments of A-431 and HSF cells were conducted using the SRB test. One hundred microliters of each cell suspension containing an exact number of cells were cultured for 24 h using 96-well plates. Following this, cells were treated with various concentrations of Bio-Ag_2ONPs (200, 20, 2, 0.2, and 0.02 µg mL^{-1}) or DMSO as a control (1 & 10%). After exposure to Bio-Ag_2ONPs for 72 h, the cells were fixed by incubating them for one hour at 4 °C. Then, 150 µL of 10% v/v trichloroacetic acid (TCA) was added after removing the growth media. Next, we discarded the solution and rinse the cells with distilled water (5X). To that end, cells were incubated with the SRB solution (70 µL, 0.4% w/v) under dark conditions for 10 min at room temperature. After incubation, all plates were rinsed thrice with acetic acid (1%) and air-dried overnight. Following this, the SRB bounded proteins were dissolved in 150 µL of Tris (10 mM) and measured at a wavelength

of 540 nm using a BMG LABTECH®-FLUOstar Omega microplate reader located in Ortenberg, Germany.

Apoptosis analysis using flow cytometry

For the flow cytometry study, we cultured A-431 cells overnight at 37 °C using a CO_2 incubator and then exposed the cells to the indicated concentration of Bio-Ag_2ONPs for 48 h. Next, all cells were washed with PBS and centrifuged (500 × *g* for 5 min at 4 °C) before discarding the supernatant and resuspending the pellets with ice-cold binding buffer to reach the targeted concentration (1×10^5 cells mL^{-1}). The tubes were placed on ice, and propidium iodide (PI), as well as annexin V-fluorescein isothiocyanate reagent, was added (1 µL of each). After a 15 min dark incubation on ice, the tubes were gently mixed with ice-cold binding buffer (400 µL). A flow cytometry study was then conducted within 30 min using an ACEA Novocyte™ flow cytometer (ACEA Biosciences Inc., San Diego, CA, USA) [139, 140].

RNA isolation and quantitative RT-PCR

After treating A-431 cells with the IC50 concentration of Bio-Ag_2ONPs, the total RNA was extracted using a commercial kit obtained from Thermo Scientific (GeneJET RNA purification kit, K0731, USA). Then, the cDNA was synthesized by a cDNA Synthesis Kit (SensiFAST™ Thermo Co., BIO-6505, America), and the subsequent expression of the indicated apoptotic genes (*Bax*, *P53*, Bcl-2, and *Cas-3*) (TableS5) were assessed by the TaqMan® Real-Time PCR Master Mix approach (Life Technologies, CA, USA) and Agilent Technologies Stratagene Mx300SP (Santa Clara, CA, USA). Gene analysis was conducted using the TaqMan probes obtained from Life Technologies (CA, USA). All genes were normalized to the reference gene 18S RNA (Life Technologies) [141, 142]. The PCR protocol was set as an initial denaturation step (95 °C for 10 min), followed by denaturation cycles (95 °C for 15 s), while the annealing/extension was set at 60 °C for 60 s.

Statistical analysis

The experimental data was performed in triplicate, and the mean values along with the standard deviation (SD) were reported. One-way analysis of variance (ANOVA) was performed using SPSS version 23 and Microsoft Excel 365 software for the experimental design and statistical analysis components of this study. The one-way ANOVA was carried out to evaluate the relationship between the measured response variable (e.g. nanoparticle production) and the various factors or independent variables investigated. This statistical technique enabled assessing the significance and impact of the different variables on the response of interest.

Conclusion

Synthesis of metal oxide nanoparticles in a biological way had proven to be effective and less toxic. The current study is the first to demonstrate *N. niacin* AUMC-B524 as an endophytic bacterium isolated from leaves of *L. shawii.* Novel biosynthetic Bio-Ag_2ONPs were successfully synthesized extracellularly by *N. niacin* AUMC-B524. Characterization results confirmed that the biosynthesized Bio-Ag_2ONPs were polydisperse, spherical, highly crystalline, and had an average size of 13.16 nm. Statistical optimization of Bio-Ag_2ONPs synthesis conditions using Placket-Burman design and Box-Behnken design demonstrated the capability to develop a high yield of abundant Bio-Ag_2ONPs. Maximum production was accomplished using the following factors: 32.5% bacterial supernatant, 5.77 mM $AgNO_3$, and a pH value of 6.77. Moreover, Bio-Ag_2ONPs exhibited high biocidal action against MDR wound pathogens, thus showing great potential to be used as an antiseptic dressing which is in high necessity for biomedical applications. Furthermore, the Bio-Ag_2ONPs demonstrated anticancer activities against the skin cancer cell line, and remarkably exhibited no cytotoxic effect on normal skin cells. This selective toxicity of Bio-Ag_2ONPs towards tumor cells compared to normal human skin fibroblast (HSF) cell lines suggests their potential application as wound dressing agents. Future research might be required to precisely identify proteins responsible for the nanoparticles synthesis and to evaluate its efficacy against tumor using in vivo model.

Supplementary Information

The online version contains supplementary material available at https://doi.org/10.1186/s12934-024-02484-0.

Supplementary Material 1. Table S1: Regression statistics and ANOVA for the actual experimental results of PBD results; Table S2: Regression statistics and ANOVA for the experimental results of BBD results; Table S3: Experimental variables for PBD to optimize biosynthesis of Ag_2ONPs at different levels; Table S4: Experimental variables for BBD to optimize biosynthesis of Ag_2ONPs at different levels; and Table S5: Primer sequences of caspase-3, *Bax* , Bcl-2 and *P53*.

Acknowledgements

The authors extend their appreciation to the Researchers Supporting Project Number (RSP2024R508), King Saud University, Riyadh, Saudi Arabia.

Author contributions

Conceptualization, Shimaa H. El-Sapagh, Nessma A. El-Zawawy and Hoda S. Nouh; methodology, Shimaa H. El-Sapagh, Nessma A. El-Zawawy and Hoda S. Nouh; software, Shimaa H. El-Sapagh, Nessma A. El-Zawawy, Hoda S. Nouh and Mostafa E. Elshobary; validation, Shimaa H. El-Sapagh, Nessma A. El-Zawawy, Hoda S. Nouh and Mostafa E. Elshobary; formal analysis, Mostafa E. Elshobary; investigation, Shimaa H. El-Sapagh, Nessma A. El-Zawawy and Hoda S. Nouh; resources, Shimaa H. El-Sapagh, Nessma A. El-Zawawy, Mostafa E. Elshobary, Mohammed Alquraishi, Hossain M. Zabed and Hoda S. Nouh; writing—original draft preparation, Shimaa H. El-Sapagh, Nessma A. El-Zawawy, Hoda S. Nouh and Mostafa E. Elshobary; writing—review and editing, Shimaa H. El-Sapagh, Nessma A. El-Zawawy, Mostafa E. Elshobary, Mohammed

Alquraishi, Hossain M. Zabed and Hoda S. Nouh; funding acquisition, Mohammed Alquraishi; All authors have read and agreed to the published version of the manuscript.

Funding
Not applicable.

Data availability
No datasets were generated or analysed during the current study.

Declarations

Ethics approval and consent to participate
Not applicable.

Consent for publication
Not applicable.

Competing interests
The authors declare no competing interests.

Received: 28 April 2024 Accepted: 17 July 2024
Published online: 06 August 2024

References

1. El-Sheekh M, Elshobary M, Abdullah E et al (2023) Application of a novel biological-nanoparticle pretreatment to Oscillatoria acuminata biomass and coculture dark fermentation for improving hydrogen production. Microb Cell Fact 22:34. https://doi.org/10.1186/s12934-023-02036-y
2. Elshobary M, Abdullah E, Abdel-Basset R et al (2024) Maximizing biofuel production from algal biomass: a study on biohydrogen and bioethanol production using Mg Zn ferrite nanoparticles. Algal Res 81:103595. https://doi.org/10.1016/j.algal.2024.103595
3. Kandathil Radhakrishnan D, AkbarAli I, Schmidt BV, John EM, Sivanpillai S, Thazhakot VS. Improvement of nutritional quality of live feed for aquaculture: an overview. Aquac Res. 2020;51:1–17. https://doi.org/10.1111/are.14357
4. Russell AD, Hugo WB. 7 antimicrobial activity and action of silver. Prog Med Chem. 1994;31:351–70. https://doi.org/10.1016/S0079-6468(08)70024-9
5. Thenmozhi M, Kannabiran K, Kumar R, Khanna VG. Antifungal activity of *Streptomyces* sp. VITSTK7 and its synthesized Ag_2O/Ag nanoparticles against medically important *Aspergillus* pathogens. J Mycol Med. 2013;23:97–103. https://doi.org/10.1016/j.mycmed.2013.04.005
6. Karunagaran V, Rajendran K, Sen S. Optimization of biosynthesis of silver oxide nanoparticles and its anticancer activity. Int J Nanosci. 2017;16:1750018.
7. Lateef A, Folarin BI, Oladejo SM, Akinola PO, Beukes LS, Gueguim-Kana EB. Characterization, antimicrobial, antioxidant, and anticoagulant activities of silver nanoparticles synthesized from *Petiveria alliacea* L. leaf extract. Prep Biochem Biotechnol. 2018;48:646–52.
8. Lateef A, Ojo SA, Akinwale AS, Azeez L, Gueguim-Kana EB, Beukes LS. Biogenic synthesis of silver nanoparticles using cell-free extract of *Bacillus* safensis LAU 13: antimicrobial, free radical scavenging and larvicidal activities. Biologia (Bratisl). 2015;70:1295–306.
9. Rashmi BN, Harlapur SF, Avinash B, Ravikumar CR, Nagaswarupa HP, Kumar MRA, et al. Facile green synthesis of silver oxide nanoparticles and their electrochemical, photocatalytic and biological studies. Inorg Chem Commun. 2020;111:107580.
10. Ahmad S, Munir S, Zeb N, Ullah A, Khan B, Ali J, et al. Green nanotechnology: a review on green synthesis of silver nanoparticles—an ecofriendly approach. Int J Nanomed. 2019. https://doi.org/10.2147/IJN.S200254.
11. Khalil AT, Khan MD, Razzaque S, Afridi S, Ullah I, Iqbal J, et al. Single precursor-based synthesis of transition metal sulfide nanoparticles and evaluation of their antimicrobial, antioxidant and cytotoxic potentials. Appl Nanosci. 2021;11:2489–502.
12. Uddin S, Bin SL, Iqbal J, Yaseen T, Laila S, Anwar S, et al. Green synthesis of nickel oxide nanoparticles using leaf extract of *Berberis* balochistanica: characterization, and diverse biological applications. Microsc Res Tech. 2021;84:2004–16.
13. Yin IX, Yu OY, Zhao IS, Mei ML, Li Q-L, Tang J, et al. Developing biocompatible silver nanoparticles using epigallocatechin gallate for dental use. Arch Oral Biol. 2019;102:106–12.
14. Wei W, Mao X, Ortiz LA, Sadoway DR. Oriented silver oxide nanostructures synthesized through a template-free electrochemical route. J Mater Chem. 2011;21:432–8.
15. Schmidt AA, Offermann J, Anton R. The role of neutral oxygen radicals in the oxidation of Ag films. Thin Solid Film. 1996;281:105–7.
16. Hou SM, Ouyang M, Chen HF, Liu WM, Xue ZQ, Wu QD, et al. Fractal structure in the silver oxide thin film. Thin Solid Film. 1998;315:322–6.
17. Her Y-C, Lan Y-C, Hsu W-C, Tsai S-Y. Effect of constituent phases of reactively sputtered AgOx film on recording and readout mechanisms of super-resolution near-field structure disk. J Appl Phys. 2004;96:1283–8.
18. Ravichandran S, Paluri V, Kumar G, Loganathan K, Kokati Venkata BR. A novel approach for the biosynthesis of silver oxide nanoparticles using aqueous leaf extract of *Callistemon* lanceolatus (myrtaceae) and their therapeutic potential. J Exp Nanosci. 2016;11:445–58.
19. Rajendran K, Sen S. Optimization of process parameters for the rapid biosynthesis of hematite nanoparticles. J Photochem Photobiol B Biol. 2016;159:82–7.
20. Rajendran K. Biological synthesis and applications of iron oxide nanoparticles. In: Karthik L, Vishnu Kirthi A, Ranjan S, Mohana Srinivasan V, editors. Biol synth nanoparticles their appl. Boca Raton: CRC Press; 2019. p. 85–92.
21. Lateef A, Ojo SA, Oladejo SM. Anti-candida, anti-coagulant and thrombolytic activities of biosynthesized silver nanoparticles using cell-free extract of Bacillus safensis LAU 13. Process Biochem. 2016;51:1406–12.
22. Rajendran K, Karunagaran V, Mahanty B, Sen S. Biosynthesis of hematite nanoparticles and its cytotoxic effect on HepG2 cancer cells. Int J Biol Macromol. 2015;74:376–81.
23. Rajendran K, Sen S, Suja G, Senthil SL, Kumar TV. Evaluation of cytotoxicity of hematite nanoparticles in bacteria and human cell lines. Coll Surf B Biointerfac. 2017;157:101–9.
24. Ovais M, Khalil AT, Ayaz M, Ahmad I, Nethi SK, Mukherjee S. Biosynthesis of metal nanoparticles via microbial enzymes: a mechanistic approach. Int J Mol Sci. 2018;19:4100.
25. Dharmaraj D, Krishnamoorthy M, Rajendran K, Karuppiah K, Jeyaraman R, Ethiraj K. Protein leakage induced marine antibiofouling activity of biosynthesized zinc oxide nanoparticles. J Clust Sci. 2021;32:643–50.
26. Vithiya K, Kumar R, Sen S. Antimicrobial activity of biosynthesized silver oxide nanoparticles. J Pure Appl Microbiol. 2014;4:3263–8.
27. Boopathi S, Gopinath S, Boopathi T, Balamurugan V, Rajeshkumar R, Sundararaman M. Characterization and antimicrobial properties of silver and silver oxide nanoparticles synthesized by cell-free extract of a mangrove-associated *Pseudomonas aeruginosa* M6 using two different thermal treatments. Ind Eng Chem Res. 2012;51:5976–85.
28. Bilal S, Khan AL, Shahzad R, Kim YH, Imran M, Khan MJ, et al. Mechanisms of Cr (VI) resistance by endophytic *Sphingomonas* sp. LK11 and its Cr (VI) phytotoxic mitigating effects in soybean (Glycine max L.). Ecotoxicol Environ Saf. 2018;164:648–58.
29. Qin S, Xing K, Jiang J-H, Xu L-H, Li W-J. Biodiversity, bioactive natural products and biotechnological potential of plant-associated endophytic actinobacteria. Appl Microbiol Biotechnol. 2011;89:457–73.
30. Jiang Y, Fang Z, Leonard W, Zhang P. Phenolic compounds in *Lycium* berry: composition, health benefits and industrial applications. J Funct Foods. 2021;77:104340.
31. Cinelli MA, Jones AD. Alkaloids of the genus *Datura*: review of a rich resource for natural product discovery. Molecules. 2021;26:2629.
32. Almoulah NF, Voynikov Y, Gevrenova R, Schohn H, Tzanova T, Yagi S, et al. Antibacterial, antiproliferative and antioxidant activity of leaf extracts of selected solanaceae species. S Afr J Bot. 2017;112:368–74.
33. El-Zawawy NA, Abou-Zeid AM, Beltagy DM, Hantera NH, Nouh HS. Mycosynthesis of silver nanoparticles from endophytic *Aspergillus* flavipes AUMC 15772: ovat-statistical optimization, characterization and biological activities. Microb Cell Fact. 2023;22:228.
34. Manikandan R, Beulaja M, Thiagarajan R, Palanisamy S, Goutham G, Koodalingam A, et al. Biosynthesis of silver nanoparticles using

aqueous extract of *Phyllanthus* acidus L. fruits and characterization of its anti-inflammatory effect against H2O2 exposed rat peritoneal macrophages. Process Biochem. 2017;55:172–81.
35. Saha N, Trivedi P, Dutta GS. Surface plasmon resonance (SPR) based optimization of biosynthesis of silver nanoparticles from rhizome extract of *Curculigo* orchioides Gaertn. and its antioxidant potential. J Clust Sci. 2016;27:1893–912.
36. Banik RM, Santhiagu A, Upadhyay SN. Optimization of nutrients for gellan gum production by sphingomonas paucimobilis ATCC-31461 in molasses based medium using response surface methodology. Bioresour Technol. 2007;98:792–7.
37. No A, Committee AM. Experimental design and optimisation (4): plackett-burman designs. Anal Method. 2013;5:1901–3.
38. Korbekandi H, Iravani S, Abbasi S. Optimization of biological synthesis of silver nanoparticles using *Lactobacillus* casei subsp casei. J Chem Technol Biotechnol. 2012;87:932–7.
39. Abdelmoneim HM, Taha TH, Elnouby MS, AbuShady HM. Extracellular biosynthesis, OVAT/statistical optimization, and characterization of silver nanoparticles (AgNPs) using leclercia adecarboxylata THHM and its antimicrobial activity. Microb Cell Fact. 2022;21:277.
40. Sidorowicz A, Fais G, Casula M, Borselli M, Giannaccare G, Locci AM, et al. Nanoparticles from microalgae and their biomedical applications. Mar Drug. 2023. https://doi.org/10.3390/md21060352.
41. Kaur N, Dey P. Bacterial exopolysaccharides as emerging bioactive macromolecules: from fundamentals to applications. Res Microbiol. 2023;174:104024.
42. Atta S, Beetz M, Fabris L. Understanding the role of AgNO 3 concentration and seed morphology in the achievement of tunable shape control in gold nanostars. Nanoscale. 2019;11:2946–58.
43. Ajitha B, Ashok Kumar Reddy Y, Sreedhara RP. Enhanced antimicrobial activity of silver nanoparticles with controlled particle size by pH variation. Powder Technol. 2015;269:110–7.
44. Ibrahim S, Ahmad Z, Manzoor MZ, Mujahid M, Faheem Z, Adnan A. Optimization for biogenic microbial synthesis of silver nanoparticles through response surface methodology, characterization, their antimicrobial, antioxidant, and catalytic potential. Sci Rep. 2021;11:770.
45. Fernando I, Zhou Y. Impact of pH on the stability, dissolution and aggregation kinetics of silver nanoparticles. Chemosphere. 2019;216:297. https://doi.org/10.1016/j.chemosphere.2018.10.122
46. Sidorowicz A, Margarita V, Fais G, Pantaleo A, Manca A, Concas A, et al. Characterization of nanomaterials synthesized from *Spirulina* platensis extract and their potential antifungal activity. PLoS ONE. 2022;17:e0274753.
47. Trivedi P, Khandelwal M, Srivastava P. Statistically optimized synthesis of silver nanocubes from peel extracts of *Citrus* limetta and potential application in waste water treatment. J Microb Biochem Technol S. 2014;4.
48. Halima R, Narula A, Sravanthi V. Optimization of process parameters for the green synthesis of silver nanoparticles using Plackett-Burman and 3-level box-behnken design. J Huazhong Univ Sci Technol. 2021;1671:4512.
49. McDonald DB, Grantham WJ, Tabor WL, Murphy MJ. Global and local optimization using radial basis function response surface models. Appl Math Model. 2007;31:2095–110.
50. Bai Y, Saren G, Huo W. Response surface methodology (RSM) in evaluation of the vitamin C concentrations in microwave treated milk. J Food Sci Technol. 2015;52:4647–51.
51. Baadhe RR, Mekala NK, Rao Parcha S, Prameela DY. Optimization of amorphadiene production in engineered yeast by response surface methodology. 3Biotech. 2014;4:317–24.
52. Quinn GP, Keough MJ. Experimental design and data analysis for biologists. Cambridge: Cambridge University Press; 2002.
53. Myers RH, Montgomery DC, Vining GG, Borror CM, Kowalski SM. Response surface methodology: a retrospective and literature survey. J Qual Technol. 2004;36:53–77.
54. Zhou J, Yu X, Ding C, Wang Z, Zhou Q, Pao H, et al. Optimization of phenol degradation by *Candida* tropicalis Z-04 using plackett-burman design and response surface methodology. J Environ Sci. 2011;23:22–30.
55. Laime-Oviedo LA, Soncco-Ccahui AA, Peralta-Alarcon G, Arenas-Chávez CA, Pineda-Tapia JL, Díaz-Rosado JC, et al. Optimization of synthesis of silver nanoparticles conjugated with *Lepechinia* meyenii (salvia) using plackett-burman design and response surface methodology—preliminary antibacterial activity. Processes. 2022;10:1727.
56. Abdelmigid HM, Morsi MM, Hussien NA, Alyamani AA, Al Sufyani NM. Comparative analysis of nanosilver particles synthesized by different approaches and their antimicrobial efficacy. J Nanomater. 2021;2021:1–12.
57. Siddiqi KS, Rashid M, Rahman A, Tajuddin HA, Rehman S. Biogenic fabrication and characterization of silver nanoparticles using aqueous-ethanolic extract of lichen (*Usnea* longissima) and their antimicrobial activity. Biomater Res. 2018;22:23.
58. Javed B, Nadhman A, Mashwani Z-R. Phytosynthesis of Ag nanoparticles from *Mentha* longifolia: their structural evaluation and therapeutic potential against HCT116 colon cancer, *Leishmanial* and bacterial cells. Appl Nanosci. 2020;10:3503–15.
59. Khandel P, Kumar Shahi S, Kanwar L, Kumar Yadaw R, Kumar SD. Biochemical profiling of microbes inhibiting silver nanoparticles using symbiotic organisms. Int J Nano Dimen. 2018;9:273.
60. Arif D, Niazi MBK, Ul-Haq N, Anwar MN, Hashmi E. Preparation of antibacterial cotton fabric using chitosan-silver nanoparticles. Fibers Polym. 2015;16:1519–26.
61. Sultan AE, AbdullahNiama HIAH. Synthesis of silver oxide nanoparticles using different precursor and study cytotoxicity against MCF-7 breast cancer cell line. Nanomed Res J. 2023;8:259–67.
62. Philip D. Rapid green synthesis of spherical gold nanoparticles using *Mangifera* indica leaf. Spectrochim Acta Part A Mol Biomol Spectrosc. 2010;77:807–10.
63. Du J, Singh H, Yi T-H. Biosynthesis of silver nanoparticles by *Novosphingobium* sp. THG-C3 and their antimicrobial potential. Artif cell Nanomed Biotechnol. 2017;45:211–7.
64. Akter S, Huq MA. Biologically rapid synthesis of silver nanoparticles by *Sphingobium* sp. MAH-11T and their antibacterial activity and mechanisms investigation against drug-resistant pathogenic microbes. Artif Cell Nanomed Biotechnol. 2020;48:672–82.
65. Muthuvel A, Adavallan K, Balamurugan K, Krishnakumar N. Biosynthesis of gold nanoparticles using *Solanum* nigrum leaf extract and screening their free radical scavenging and antibacterial properties. Biomed Prev Nutr. 2014;4:325–32.
66. Amin ZR, Khashyarmanesh Z, Bazzaz BSF, Noghabi ZS. Does biosynthetic silver nanoparticles are more stable with lower toxicity than their synthetic counterparts? Iran J Pharm Res IJPR. 2019;18:210.
67. Saeb ATM, Alshammari AS, Al-Brahim H, Al-Rubeaan KA. Production of silver nanoparticles with strong and stable antimicrobial activity against highly pathogenic and multidrug resistant bacteria. Sci world J. 2014;2014:704708.
68. Rather M, Pandian KJ, Sundarapandian SM, Yogamoorthi A. Biosynthesis and characterization of silver nanoparticles using leaf extract of *Wedelia* urticifolia (blume) DC and evaluation of antibacterial efficacy. IOSR J Pharm Biol Sci. 2017;12:14–23.
69. Anandalakshmi K, Venugobal J, Ramasamy V. Characterization of silver nanoparticles by green synthesis method using *Pedalium* murex leaf extract and their antibacterial activity. Appl Nanosci. 2016;6:399–408.
70. Rautela A, Rani J. Green synthesis of silver nanoparticles from *Tectona* grandis seeds extract: characterization and mechanism of antimicrobial action on different microorganisms. J Anal Sci Technol Springer. 2019;10:1–10.
71. Stoehr LC, Gonzalez E, Stampfl A, Casals E, Duschl A, Puntes V, et al. Shape matters: effects of silver nanospheres and wires on human alveolar epithelial cells. Part Fibre Toxicol. 2011;8:1–15.
72. Elemike EE, Onwudiwe DC, Ekennia AC, Jordaan A. Synthesis and characterisation of silver nanoparticles using leaf extract of *Artemisia* afra and their in vitro antimicrobial and antioxidant activities. IET Nanobiotechnol. 2018;12:722–6.
73. Gurunathan S, Qasim M, Park C, Yoo H, Kim JH, Hong K. Cytotoxic potential and molecular pathway analysis of silver nanoparticles in human colon cancer cells HCT116. Int J Mol Sci. 2018;19:2269.
74. Swidan NS, Hashem YA, Elkhatib WF, Yassien MA. Antibiofilm activity of green synthesized silver nanoparticles against biofilm associated enterococcal urinary pathogens. Sci Rep. 2022;12:3869.

75. Choi M, Shin K-H, Jang J. Plasmonic photocatalytic system using silver chloride/silver nanostructures under visible light. J Coll Interfac Sci. 2010;341:83–7.
76. Porramezan M, Eisazadeh H. Fabrication and characterization of polyaniline nanocomposite modified with Ag2O nanoparticles. Compos Part B Eng. 2011;42:1980–6.
77. Harroun SG, Zhang Y, Chen TH, Chang HT, Vallée-Bélisle A. Silver oxide model surface improves computational simulation of surface-enhanced Raman spectroscopy on silver nanoparticles. Phys Chem Chem Phys. 2021;23:15480–4.
78. Ayanwale AP, Estrada-Capetillo BL, Reyes-López SY. Evaluation of antifungal activity by mixed oxide metallic nanocomposite against *Candida* spp. Processes. 2021;9:773.
79. Waterhouse GIN, Bowmaker GA, Metson JB. The thermal decomposition of silver (I, III) oxide: a combined XRD, FT-IR and Raman spectroscopic study. Phys Chem Chem Phys. 2001;3:3838–45.
80. Panáček A, Kvitek L, Prucek R, Kolář M, Večeřová R, Pizúrová N, et al. Silver colloid nanoparticles: synthesis, characterization, and their antibacterial activity. J Phys Chem B ACS Publ. 2006;110:16248–53.
81. Shrivastava S, Bera T, Roy A, Singh G, Ramachandrarao P, Dash D. Retracted: characterization of enhanced antibacterial effects of novel silver nanoparticles. Nanotechnology. 2007;18:225103.
82. Bakhtiari-Sardari A, Mashreghi M, Eshghi H, Behnam-Rasouli F, Lashani E, Shahnavaz B. Comparative evaluation of silver nanoparticles biosynthesis by two cold-tolerant *Streptomyces* strains and their biological activities. Biotechnol Lett. 2020;42:1985–99.
83. Singh R, Wagh P, Wadhwani S, Gaidhani S, Kumbhar A, Bellare J, et al. Synthesis, optimization, and characterization of silver nanoparticles from *Acinetobacter* calcoaceticus and their enhanced antibacterial activity when combined with antibiotics. Int J Nanomed. 2013. https://doi.org/10.2147/IJN.S48913.
84. Zhang M, Zhang K, De Gusseme B, Verstraete W, Field R. The antibacterial and anti-biofouling performance of biogenic silver nanoparticles by *Lactobacillus* fermentum. Biofouling. 2014;30:347–57.
85. Meire MA, Coenye T, Nelis HJ, De Moor RJG. Evaluation of Nd: YAG and Er: YAG irradiation, antibacterial photodynamic therapy and sodium hypochlorite treatment on *Enterococcus* faecalis biofilms. Int Endod. 2012;45:482–91.
86. Martínez-Castañón GA, Niño-Martínez N, Martínez-Gutierrez F, Martínez-Mendoza JR, Ruiz F. Synthesis and antibacterial activity of silver nanoparticles with different sizes. J Nanoparticle Res. 2008;10:1343–8.
87. Gudkov SV, Serov DA, Astashev ME, Semenova AA, Lisitsyn AB. Ag2O nanoparticles as a candidate for antimicrobial compounds of the new generation. Pharmaceuticals. 2022;15:968.
88. T. Galatage S, S. Hebalkar A, V. Dhobale S, R. Mali O, S. Kumbhar P, V. Nikade S, et al. Silver nanoparticles: properties, synthesis, characterization, applications and future trends. Silver Micro-Nanoparticles - Prop Synth Charact Appl. IntechOpen. 2021. https://www.intechopen.com/books/silver-micro-nanoparticles-properties-synthesis-characterization-and-applications/silver-nanoparticles-properties-synthesis-characterization-applications-and-future-trends
89. Tavares TD, Antunes JC, Padrão J, Ribeiro AI, Zille A, Amorim MTP, et al. Activity of specialized biomolecules against gram-positive and gram-negative bacteria. Antibiotics. 2020;9:314.
90. Loo YY, Rukayadi Y, Nor-Khaizura MAR, Kuan CH, Chieng BW, Nishibuchi M, et al. In vitro antimicrobial activity of green synthesized silver nanoparticles against selected gram-negative foodborne pathogens. Front Microbiol Front. 2018;9:379304.
91. Joshi AS, Singh P, Mijakovic I. Interactions of gold and silver nanoparticles with bacterial biofilms: molecular interactions behind inhibition and resistance. Int J Mol Sci. 2020;21:7658.
92. Singh P, Pandit S, Mokkapati V, Garnæs J, Mijakovic I. A sustainable approach for the green synthesis of silver nanoparticles from *Solibacillus* isronensis sp and their application in biofilm inhibition. Molecules. 2020;25:2783.
93. Das B, Dash SK, Mandal D, Ghosh T, Chattopadhyay S, Tripathy S, et al. Green synthesized silver nanoparticles destroy multidrug resistant bacteria via reactive oxygen species mediated membrane damage. Arab J Chem. 2017;10:862–76.
94. Bin-Jumah M, Al-Abdan M, Albasher G, Alarifi S. Effects of green silver nanoparticles on apoptosis and oxidative stress in normal and cancerous human hepatic cells in vitro. Milton Park: Taylor & Francis; 2020. p. 1537–48.
95. Makvandi P, Baghbantaraghdari Z, Zhou W, Zhang Y, Manchanda R, Agarwal T, et al. Gum polysaccharide/nanometal hybrid biocomposites in cancer diagnosis and therapy. Biotechnol Adv. 2021;48:107711.
96. Elmore S. Apoptosis: a review of programmed cell death. Toxicol Pathol. 2007;35:495–516.
97. Ali SS, Morsy R, El-Zawawy NA, Fareed MF, Bedaiwy MY. Synthesized zinc peroxide nanoparticles (ZnO2-NPs): a novel antimicrobial, anti-elastase, anti-keratinase, and anti-inflammatory approach toward polymicrobial burn wounds. Milton Park: Taylor & Francis; 2017. p. 6059–73.
98. Jena P, Mohanty S, Mallick R, Jacob B, Sonawane A. Toxicity and antibacterial assessment of chitosancoated silver nanoparticles on human pathogens and macrophage cells. Milton Park: Taylor & Francis; 2012. p. 1805–18.
99. Jeyaraj M, Sathishkumar G, Sivanandhan G, MubarakAli D, Rajesh M, Arun R, et al. Biogenic silver nanoparticles for cancer treatment: an experimental report. Coll Surfac B Biointerfac. 2013;106:86–92.
100. Hanahan D, Weinberg RA. The hallmarks of cancer. Cell. 2000;100:57–70.
101. Plati J, Bucur O, Khosravi-Far R. Dysregulation of apoptotic signaling in cancer: molecular mechanisms and therapeutic opportunities. J Cell Biochem. 2008;104:1124–49.
102. Jan R. Understanding apoptosis and apoptotic pathways targeted cancer therapeutics. Adv Pharm Bull. 2019;9:205.
103. Li T, Kon N, Jiang L, Tan M, Ludwig T, Zhao Y, et al. Tumor suppression in the absence of p53-mediated cell-cycle arrest, apoptosis, and senescence. Cell. 2012;149:1269–83.
104. Guo X-X, Li Y, Sun C, Jiang D, Lin Y-J, Jin F-X, et al. p53-dependent Fas expression is critical for ginsenoside Rh2 triggered caspase-8 activation in HeLa cells. Prot Cell. 2014;5:224–34.
105. Liao C, Li Y, Tjong SC. Bactericidal and cytotoxic properties of silver nanoparticles. Int J Mol Sci. 2019;20:449.
106. Kwan YP, Saito T, Ibrahim D, Al-Hassan FMS, Ein Oon C, Chen Y, et al. Evaluation of the cytotoxicity, cell-cycle arrest, and apoptotic induction by Euphorbia hirta in MCF-7 breast cancer cells. Pharm Biol. 2016;54:1223–36.
107. Oves M, Aslam M, Rauf MA, Qayyum S, Qari HA, Khan MS, et al. Antimicrobial and anticancer activities of silver nanoparticles synthesized from the root hair extract of Phoenix dactylifera. Mater Sci Eng C. 2018;89:429–43.
108. AshaRani PV, Low Kah Mun G, Hande MP, Valiyaveettil S. Cytotoxicity and genotoxicity of silver nanoparticles in human cells. ACS Nano. 2009;3:279–90.
109. Ahmed KBR, Nagy AM, Brown RP, Zhang Q, Malghan SG, Goering PL. Silver nanoparticles: significance of physicochemical properties and assay interference on the interpretation of in vitro cytotoxicity studies. Toxicol Vitr. 2017;38:179–92.
110. Kumar A, Singh R, Yadav A, Giri DD, Singh PK, Pandey KD. Isolation and characterization of bacterial endophytes of *Curcuma* longa L. 3 Biotech. 2016;6:1–8.
111. Ameen F, AlYahya S, Govarthanan M, ALjahdali N, Al-Enazi N, Alsamhary K, et al. Soil bacteria *Cupriavidus* sp. mediates the extracellular synthesis of antibacterial silver nanoparticles. J Mol Struct. 2020;1202:127233.
112. El-Sapagh S, El-Shenody R, Pereira L, Elshobary M. Unveiling the potential of algal extracts as promising antibacterial and antibiofilm agents against multidrug-resistant *Pseudomonas aeruginosa*: in vitro and in silico studies including molecular docking. Plants. 2023;12:3324. https://doi.org/10.3390/plants12183324
113. Huo S, Basheer S, Liu F, Elshobary M, Zhang C, Qian J, et al. Bacterial intervention on the growth, nutrient removal and lipid production of filamentous oleaginous microalgae *Tribonema* sp. Algal Res. 2020;52:102088. https://doi.org/10.1016/j.algal.2020.102088
114. Manikprabhu D, Kjj L. Antibacterial activity of silver nanoparticles against methicillin-resistant *Staphylococcus* aureus synthesized using model *Streptomyces* sp. pigment by photo-irradiation method. J Pharm Res. 2013;6:255–60.
115. Sunkar S, Nachiyar CV. Biogenesis of antibacterial silver nanoparticles using the endophytic bacterium *Bacillus* cereus isolated from *Garcinia* xanthochymus. Asian Pac J Trop Biomed. 2012;2:953–9.
116. Plackett RL, Burman JP. The design of optimum multifactorial experiments. Biometrika. 1946;33:305–25.

117. Talukdar S, Talukdar M, Buragohain M, Yadav A, Yadav RNS, Bora TC. Enhanced candicidal compound production by a new soil isolate Penicillium verruculosum MKH7 under submerged fermentation. BMC Microbiol. 2016;16:1–12.
118. Al-Sarrani AQM, El-Naggar MYM. Application of Plackett-Burman factorial design to improve citrinin production in *Monascus* ruber batch cultures. Bot Stud. 2006;47:167–74.
119. El-Naggar NEA, Mohamedin A, Hamza SS, Sherief AD. Extracellular biofabrication, characterization, and antimicrobial efficacy of silver nanoparticles loaded on cotton fabrics using newly isolated *Streptomyces* sp. SSHH-1E. J Nanomater. 2016. https://doi.org/10.1155/2016/3257359.
120. Box GEP, Behnken DW. Some new three level designs for the study of quantitative variables. Technometrics. 1960;2:455–75.
121. Arul Jose P, Sivakala KK, Jebakumar SRD. Formulation and statistical optimization of culture medium for improved production of antimicrobial compound by *Streptomyces* sp. JAJ06. Int J Microbiol. 2013. https://doi.org/10.1155/2013/526260.
122. Roy S, Mukherjee T, Chakraborty S, Das TK. Biosynthesis, characterisation & antifungal activity of silver nanoparticles synthesized by the fungus *Aspergillus* foetidus MTCC8876. Dig J Nanomater Biostructures. 2013;8:197–205.
123. Zhang XF, Liu ZG, Shen W, Gurunathan S. Silver nanoparticles: synthesis, characterization, properties, applications, and therapeutic approaches. Int J Mol Sci. 2016;17:1534.
124. Wypij M, Jędrzejewski T, Trzcińska-Wencel J, Ostrowski M, Rai M, Golińska P. Green synthesized silver nanoparticles: antibacterial and anticancer activities, biocompatibility, and analyses of surface-attached proteins. Front Microbiol Front. 2021;12:632505.
125. Senousy HH, Khairy HM, El-Sayed HS, Sallam ER, El-Sheikh MA, Elshobary ME. Interactive adverse effects of low-density polyethylene microplastics on marine microalga *Chaetoceros* calcitrans. Chemosphere. 2023;311:137182. https://doi.org/10.1016/j.chemosphere.2022.137182
126. Ottoni CA, Simões MF, Fernandes S, Dos Santos JG, Da Silva ES, de Souza RFB, et al. Screening of filamentous fungi for antimicrobial silver nanoparticles synthesis. Amb Expr. 2017;7:1–10.
127. Majumdar R, Bag BG, Maity N. Acacia nilotica (Babool) leaf extract mediated size-controlled rapid synthesis of gold nanoparticles and study of its catalytic activity. Int Nano Lett. 2013;3:1–6.
128. Agressott EVH, Blätte D, Cunha FA, Noronha VT, Ciesielski R, Hartschuh A, et al. Vibrational spectroscopy and morphological studies on protein-capped biosynthesized silver nanoparticles. ACS Omega. 2020;5:386–93.
129. Perez C. Antibiotic assay by agar-well diffusion method. Acta Biol Med Exp. 1990;15:113–5.
130. Pal S, Tak YK, Song JM. Does the antibacterial activity of silver nanoparticles depend on the shape of the nanoparticle? a study of the gram-negative bacterium *Escherichia* coli. Appl Environ Microbiol Am Soc Microbiol. 2007;73:1712–20.
131. El-Zawawy NA, Kenawy ER, Ahmed S, El-Sapagh S. Bioproduction and optimization of newly characterized melanin pigment from Streptomyces djakartensis NSS-3 with its anticancer, antimicrobial, and radioprotective properties. Microb Cell Fact. 2024;23:23.
132. Pereira E, Cadavez V, Barros L, Encina-Zelada C, Stojković D, Sokovic M, et al. Chenopodium quinoa Willd. (quinoa) grains: a good source of phenolic compounds. Food Res Int. 2020;137:109574.
133. Soković M, Glamočlija J, Marin PD, Brkić D, Van Griensven LJLD. Antibacterial effects of the essential oils of commonly consumed medicinal herbs using an in vitro model. Molecules. 2010;15:7532–46.
134. El-Zawawy NA, Ali SS, Khalil MA, Sun J, Nouh HS. Exploring the potential of benzoic acid derived from the endophytic fungus strain *Neurospora* crassa SSN01 as a promising antimicrobial agent in wound healing. Microbiol Res. 2022;262:127108.
135. May J, Shannon K, King A, French G. Glycopeptide tolerance in *Staphylococcus aureus*. J Antimicrob Chemother. 1998;42:189–97.
136. Guggenbichler JP, Semenitz E, König P. Kill kinetics and regrowth pattern of bacteria exposed to antibiotic concentrations simulating those observed in vivo. J Antimicrob Chemother. 1985;15:139–46.
137. Zainin NS, Lau KY, Zakaria M, Son R, Razis AFA, Rukayadi Y. Antibacterial activity of Boesenbergia rotunda (L.) Mansf. A. extract against Escherichia coli. Int Food Res J. 2013;20:3319.
138. Thakare R, Singh AK, Das S, Vasudevan N, Jachak GR, Reddy DS, et al. Repurposing Ivacaftor for treatment of *Staphylococcus* aureus infections. Int J Antimicrob Agent. 2017;50:389–92.
139. Fekry MI, Ezzat SM, Salama MM, Alshehri OY, Al-Abd AM. Bioactive glycoalkaloides isolated from *Solanum* melongena fruit peels with potential anticancer properties against hepatocellular carcinoma cells. Sci Rep. 2019;9:1746.
140. Bashmail HA, Alamoudi AA, Noorwali A, Hegazy GA, AJabnoor G, Choudhry H, et al. Thymoquinone synergizes gemcitabine anti-breast cancer activity via modulating its apoptotic and autophagic activities. Sci Rep. 2018;8:11674.
141. Yang J, Sun J, Yan Y. lip 2, a novel lipase gene cloned from *Aspergillus* niger exhibits enzymatic characteristics distinct from its previously identified family member. Biotechnol Lett. 2010;32:951–6.
142. Yu J, Mohawed SM, Bhatnagar D, Cleveland TE. Substrate-induced lipase gene expression and aflatoxin production in *Aspergillus* parasiticus and *Aspergillus* flavus. J Appl miCrobiol. 2003;95:1334–42.

Publisher's Note